Copper isotope method development for determining the source of mineralised provinces

Thesis submitted in accordance with the requirements of the University of Adelaide for an Honours Degree in Geology

Christopher Richard Lowczak

November 2019

THE UNIVERSITY of ADELAIDE

TITLE

Copper isotope method development for determining the source of mineralised provinces

RUNNING TITLE

Cu isotopes method development for determining the source of mineralised provinces

ABSTRACT

Many isotope proxies have been applied to study the prosperous iron oxide copper gold (IOCG) province in the eastern Gawler Craton (E.G.C) and Au mineralised region of the cental Gawler Craton (C.G.C), in Southern Australia. Yet, copper isotope proxies- an indicator for low temperature fluid flow and sulfide mineralisation- have yet to be applied to the region. In this study, purification techniques using automatic column chromatography were demonstrated during separation of Cu from matrix elements. Cu isotopes – ^{65}Cu & ^{63}Cu – were used to understand the extent of mantle input and mantle metasomatism, potentially responsible for the Cu in IOCG mineralisation. Eleven samples were gathered. Three mafic enclaves and four intrusives from Central Gawler Gold Province and four intrusives from eastern Gawler IOCG province. Separation using automatic column chromatography proved challenging, with matrix elements abundant throughout the purified fractions (Co, Ti, Fe, Mg, Na), due to poor separation. Ti proved to a major interferent during isotopic analysis using a Multicollector-ICP-MS, positively offsetting values. E.C.G samples showed the most positively fractionated $\delta^{65}Cu$ values (+0.69 ± 0.024‰ to +1.422 ± 0.077‰). Enclaves from the C.G.C showed the most negatively fractionated $\delta^{65}Cu$ values (-0.053 ± 0.023‰ to -0.897 ± 0.006‰), while intrusives from this region showed more positive $\delta^{65}Cu$ values (+0.084±0.23‰ to +0.397±0.011‰). All samples showed a lack of hydrothermal alteration. Magmatic sulphide containing E.G.C samples had the most positive $\delta^{65}Cu$ values; which cannot be explained by current understanding of Cu isotope fractionation during sulfide saturation. This trend may instead be attributed to a heterogeneous sub-continental lithospheric mantle (SCLM) source. In contrast the negative $\delta^{65}Cu$ values of mafic enclaves is

possibly caused by assimilation of S-type granitic crust and/or possibly due to a heterogeneous SCLM source.

KEYWORDS

IOCG, copper isotope, copper isotope fractionation, mantle metasomatism, automatic column chromatography, separation techniques for silicate matrices

TABLE OF CONTENTS

LIST OF FIGURES AND TABLES

INTRODUCTION

As the global demand for copper continues to rise, exploration for copper is becoming increasingly more challenging because the majority of easily explored resources have already been discovered. Successful exploration increasingly hinges on the development of new approaches and novel techniques. Across Australia, Archean and Proterozoic terranes - such as the Yilgarn craton, North Australian craton, Gawler Craton and Mount Isa terrane – are host to significant mineral deposits and are important regions for past, present and future mineral exploration (Hand, Reid, & Jagodzinski, 2007).

The Gawler Craton is an extensive Archean to Mesoproterozoic crystalline basement located in Southern Australia host to the world class Olympic Dam Fe-Oxide Cu-Au-U-REE (rare earth element) deposit. Olympic Dam is one of the world's most significant Cu and Au deposit, containing 10.4 billion tonnes at 0.77 wt.% Cu, 0.32 g/T Au, as well as 0.25 kg/t U_3O_8 (Skirrow, Wielen, Champion, Czarnota, & Thiel, 2018), making it the single largest known U deposit in the world (Skirrow, Bastrakov, Barovich, Fraser, Creaser *et al.*, 2007; Skirrow *et al.*, 2018). The region is also host to numerous other synchronous iron oxide copper gold (IOCG) deposits, including; Prominent Hill, Carrapateena, Moonta-Wallaroo and Hillside. These deposits, located on the eastern margin of the Gawler Craton, collectively form the Olympic IOCG belt (Skirrow *et al.*, 2018). In addition to IOCG-style mineralisation, the central Gawler Craton is host to Au-rich deposits (Hand *et al.*, 2007), some of which include; Tarcoola, Barnes, Paris, Tunkillia (Figure 1).

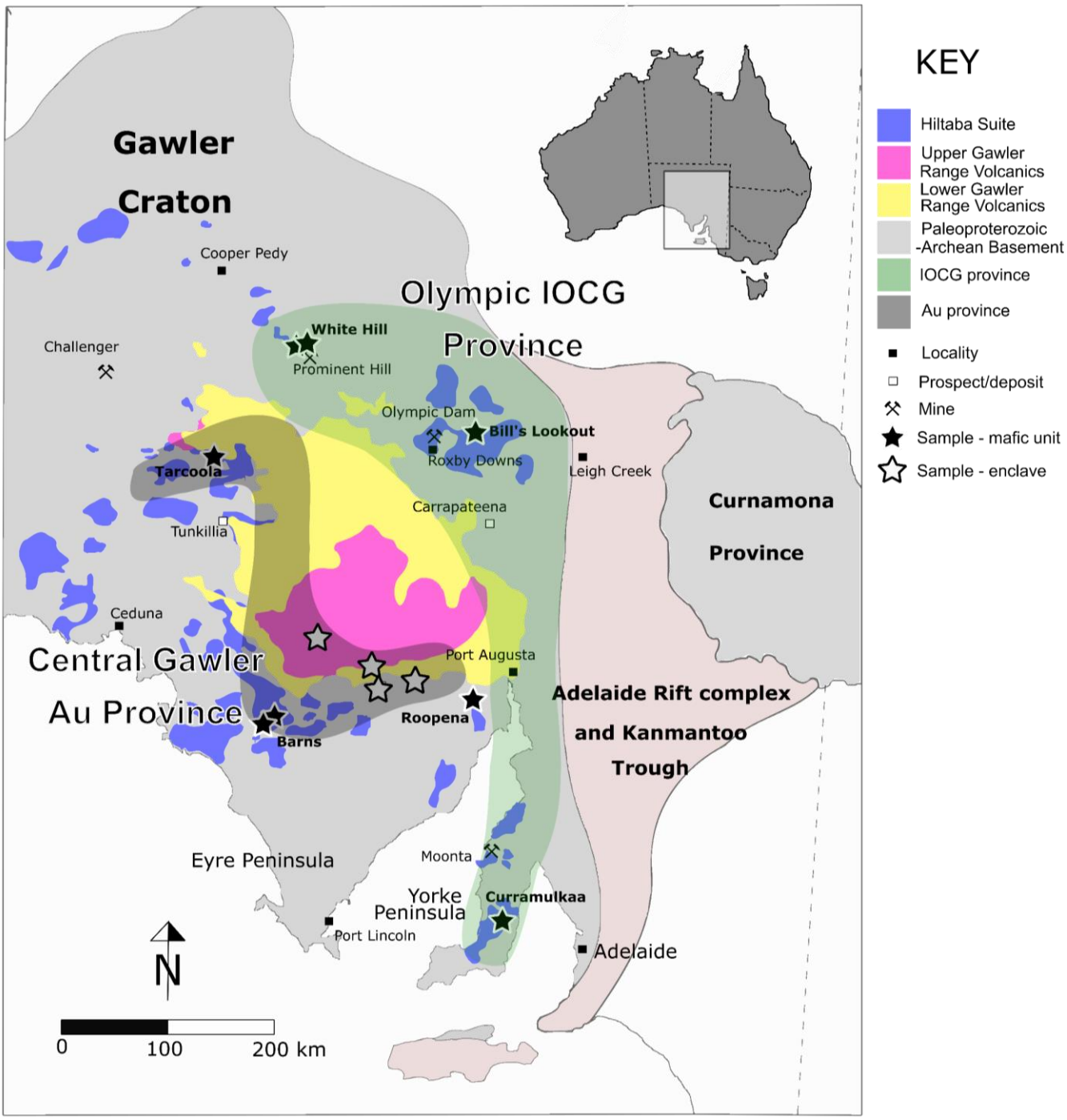

Figure 1: Simplified geology map of the Mesoproterozoic Silicic Large Igneous Province in the Gawler Craton, Southern Australia, showing the Gawler Range Volcanics (GRV), Hiltaba Suite (HS), two main mineralized regions of the Craton, and notable deposits and mines within the region. Samples analysed from the central Gawler Craton and eastern Gawler Craton are shown. Adapted from (McAvaney and Wade, 2015).

Gawler Range Volcanics–Hiltaba Suite

The Gawler Range Volcanics (GRV) is thought to be co-magmatic with the Hiltaba Suite (HS) which is also located in the Gawler Craton. The GRV-HS magmatic event represents one of the largest felsic igneous events in the world and, at present, covers more than 25 000 km^2 of the central Gawler Craton to form a felsic-dominant Large Igneous Province (LIP) (Allen, McPhie, Ferris, & Simpson, 2008; Hand *et al.*, 2007) (Figure 1). The GRV-HS magmatic event occurred in an intercontinental setting during the assembly of the Laurentian supercontinent during the Mesoproterozoic (Hand *et al.*, 2007). This event was the final tectonothermal period in the development of the Gawler Craton (Allen, Simpson, McPhie, & Daly, 2003).

It is largely agreed that the GRV-HS magmatism was the thermal driver for crustal-scale fluid circulation which gave rise to the Cu-Ag-U-REE mineralisation in the Olympic IOCG province and synchronous Au mineralisation of the central Gawler Craton (Hand *et al.*, 2007; Motta, Betts, Thiel, Curtis, Armit *et al.*, 2019; Wade, Payne, & Reid, 2019).

The spatial relationship of these granites has been the topic of much research. Geochemical evidence suggests that the Hiltaba Suite Granites, which are associated with IOCG systems in the Eastern Gawler Craton, are more evolved and rich in U and Th compared to the Hiltaba Suite Granites , in the centre Gawler Craton, which are associated with Au-rich mineral systems (Foden & Stewart, 2003). Furthermore, a significant difference in heat flow is observed at present between the IOCG province

(90 ± 10 mWm^{-2}) and the Au dominated province (54 ± 5 mWm^{-2}), to indicate that the lithologies within each province are compositionally distinct from one another (Hand *et al.*, 2007)

Cu Isotope Fractionation

The ratio of the two stable isotopes of copper – ^{63}Cu and ^{65}Cu – expressed as $\delta^{65}Cu$ (relative to standard reference material – NIST 976), is a novel proxy in tracing crustal, and crust-mantle processes. The study of $\delta^{65}Cu$ in both whole rock and minerals has been successfully applied to numerous locations and a variety of geological settings (Lee, Luffi, Chin, Bouchet, Dasgupta *et al.*, 2012; Li, Jackson, Pearson, Alard, & Chappell, 2009 ; S. A. Liu, Huang, Wörner, Yang, Tang *et al.*, 2015; Mathur, Titley, Barra, Brantley, Wilson *et al.*, 2009; Y.-C. Zheng, Liu, Wu, Griffin, Li *et al.*, 2019).

$\delta^{65}Cu$ values can be negative or positive with many studies showing that datasets cluster around zero, making processes that cause this value to be other than zero easily recognised. Early studies, such as those conducted by Mathur *et al.* (2009) and Li *et al.* (2010), lead to important developments in the use of these isotopes as a proxy for tracing fluid pathways and the sources of copper in porphyry deposits. For example, Li *et al.* (2010) demonstrated direct correlation between different zones within the porphyry Cu-Au system at Northparkes, NSW, Australia, to the copper isotopic values of secondary Cu-sulfide minerals. Li *et al.* (2010) concluded that copper isotopes generally trend towards negative $\delta^{65}Cu$ values with increasing distance from the core. With secondary sulphides containing a positive $\delta^{65}Cu$ signature (Figure 2).

In recent years, the concept of copper isotope fractionation has been applied to magmatic differentiation processes, further deepening the knowledge of fluid pathways for mineral deposits as well as estimates for the compositions of the silicate Earth. Liu *et al.* (2015) applied this knowledge to deeper igneous systems involving crust-mantle differentiation processes. Their data indicates that metsasomatised peridotites exhibit the highest variability in δ^{65}Cu with values ranging from –0.64 to +1.82‰, in comparison to unmetasomatised peridotites which have a much narrower range of –0.15 to +0.18‰ (Figure 2). In contrast, Mid-Oceanic Ridge Basalts (MORB) and Ocean Island Basalts (OIB) have homogenous δ^{65}Cu values otherwise indistinguishable from those of the unmetasomatised peridotite. This leads to suggest that metasomatism is capable of substantially fractionating Cu in rocks to higher δ^{65}Cu values. Furthermore, it is interpreted that partial melting has little effect on fractionation such that δ^{65}Cu in mantle-derived magmas serves as a record of their mantle source, more specifically the degree to which their mantle source(s) was metasomatised by fluids (S. A. Liu *et al.*, 2015; Mathur *et al.*, 2009).

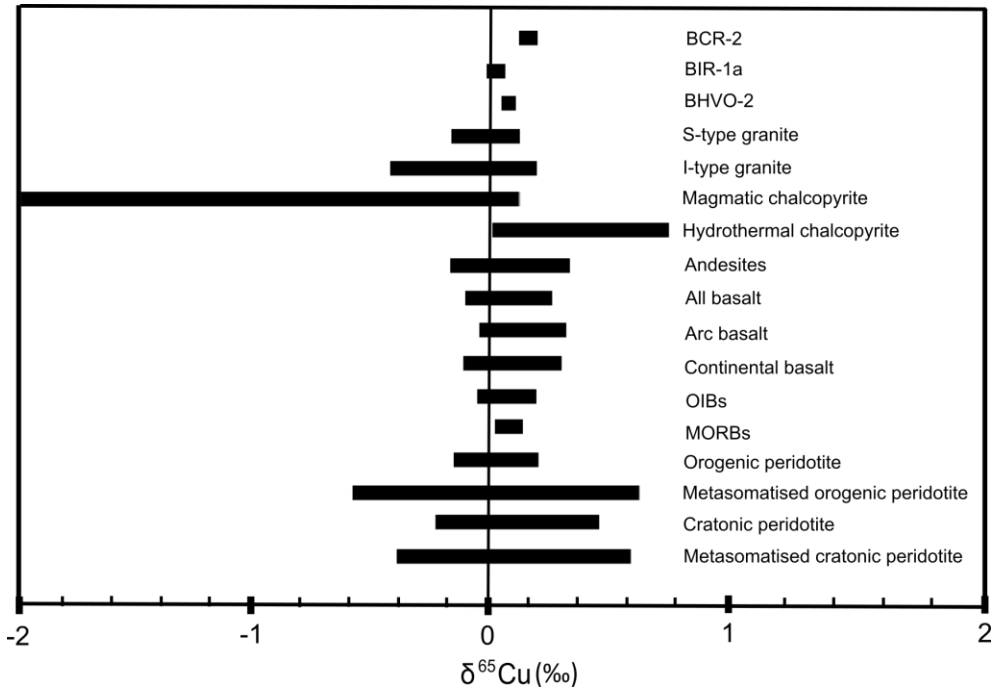

Figure 2 The δ^{65}Cu values of various geological reservoirs adapted from (Liu *et al.* 2015).

The source of copper responsible for the IOCG mineralisation within the Gawler Craton is thought to correlate with the level of mineralisation. Minor IOCG systems have been shown to have a substantial crustal source of REE, which can be distinguished from the giant Olympic Dam deposit, which exhibits greater mantle source of REE and ore-forming elements (Skirrow *et al.*, 2007). Nevertheless, the formation of the Olympic IOCG province has been suggested to relate to the foundering of previously fertilized and metasomatised lithospheric mantle (Skirrow *et al.*, 2018). Therefore understanding the copper isotope geochemistry of the mafics within the Gawler Craton can help constrain the source of copper in the ore-forming fluids (i.e. mantle vs. crustal source) and help improve our understanding of the spatial relationship between mineral systems in the Gawler Craton.

Method development

The chemical separation of Cu and other transition metals from matrix elements generally requires manual column chromatography and the measurement of resulting solutions on a multi collector-inductively coupled plasma mass spectrometer (MC-ICP-MS). Although replicable techniques have been developed, these are often time consuming and require constant attention and must be calibrated for each matrix/ sample type of interest (Sossi, Halverson, Nebel, & Eggins, 2014). Automated techniques have been successfully developed and implemented in numerous disciplines utilizing isotope analysis, including continuous-flow gas-source isotope ratio mass spectrometry and noble gas spectrometry. Furthermore, recent methods have been developed for the use of automated column chromatography in the separation of Sr and Ca from silicate-matrices (Romaniello, Field, Smith, Gordon, Kim *et al.*, 2015), however such methods are yet to be developed for Cu. The automation of the element separation via column chromatography has many advantages to traditional manual techniques, including; reduced analytical cost, the possible decrease in human induced errors and most importantly faster sample processing (Enge, Field, Jolley, Ecroyd, Kim *et al.*, 2016). From a resource and industry perspective, fast data collection has the benefit of reducing expenditure and making such techniques commercially available.

The principal aims of this study are twofold: (1) To develop a novel, fully automated Cu separation method using the prepFAST MC. More specifically to develop a fully automated, low pressure chromatography (<100 psi) system from silica matrices from the chosen field sites, in a commercially available and easily reproducible manner.

Following on, to demonstrate the application of this procedure in conjunction with manual chromatography methods. (2) To further understand the extent of mantle input to the IOCG mineralisation in the Gawler Craton and to better resolve the spatial arrangement of mineralisation. This will be achieved by studying the copper isotopic signatured of mafic units within both mineralised provinces. These aims fit with the primary objective of understanding the method of copper enrichment within IOCG systems using copper isotopes as a proxy for metasomatic processes. The outcomes of this study will aid the development of new, geochemical exploration techniques such as the ability to assess magmas fertility in under-explored provinces using Cu isotopes.

GEOLOGICAL BACKGROUND

Geological Setting

The Gawler Craton was dominated by two phases of activity, the first occurring during the Late Archean (ca. 2550–2500 Ma) and the second, during the late Paleoproterozoic to early Mesozoic (ca. 1900–1450 Ma). Between these events, the Gawler Craton remained largely stable. During the early Mesozoic, the Gawler Craton experienced multiple phases of local magmatic events. The first occurred at ca. 2000 Ma and the second at ca. 1850 Ma during the Cornian orogeny, before its termination around 1730 to 1690 Ma by the Kimban Orogeny. The Kimban Orogeny was followed by renewed extension and the subsequent emplacement of magmatic suites such as the likely arc-related, juvenile St. Peter Suite (ca. 1620–1610 Ma). This was followed by the voluminous and predominantly felsic magmatic event of the Gawler Range Volcanics (GRV) (ca. 1592 Ma) and coeval Hiltaba Suite (HS) event (1597–1579 Ma) (Hand *et*

al., 2007; Reid & Payne, 2017; Wade *et al.*, 2019). This magmatic event temporally overlaps the IOCG, Au, and Ag-Pb-Zn mineralisation seen in the eastern, central and southern central Gawler Craton, respectively (Wade *et al.*, 2019).

The Gawler Range Volcanics (GRV) are divided into lower and upper sequences (Wade *et al.*, 2019). The upper GRV is characterised by highly voluminous, flat lying and undeformed felsic rocks ranging in composition from dacite and rhyodacite to rhyolite. The lower, less voluminous sequence, is characterised by a wide range of compositions, comprising of moderately dipping basalt, andesite, dacite, rhyodacite, rhyolite lavas and pyroclastic rocks (Allen *et al.*, 2008; Hand *et al.*, 2007; Wade *et al.*, 2019). The long lasting intrusive event of the Hiltaba Suite was bimodal, however predominantly granitic in composition (Wade *et al.*, 2019). Subsurface exposures in addition to geophysical interpretations suggest the Hiltaba Suite spans an area of 30 000 km^2 (Wade *et al.*, 2019). Mafic components within the suite are less common and mainly observed from drill core.

Geochemisty

This study focuses on a suite of mafic rocks from the GRV-HS mafic units, which are interpreted to represent the most primitive melts within these suites. Despite assuming a mantle source, the possibility of crustal contamination must also be considered. The $\varepsilon Nd_{1590\ Ma}$ range (–7.0 – 2.5) of basalts within the lower GRV and their enrichment in high field strength elements (HFSE) suggests the GRV magmas likely assimilated some older crust. The Rhyolites of the lower GRV show similar $\varepsilon Nd_{1590\ Ma}$ values (–7.0 – 1.2) and are enriched in REE, Y, HFSE, Rb and F. The upper GRV igneous units have

$\varepsilon Nd_{1590\ Ma}$ values within the range of (–5.4 to –1.8) and show enrichment in HFSE and REE, to suggest a greater crustal component in these magmas than in the lower GRV (Wade *et al.*, 2019).

The Hiltaba Suite granites are geochemically more variable, however this variation largely arises from fractionation processes of primary magmas. The Hiltaba Suite is enriched in HFSE, REE, U, Th and K (Wade *et al.*, 2019). The granites associated with the IOCG mineralisation in the Eastern margin of the Gawler Craton are more fractionated, metaluminous, oxidised, enriched in Rb and HFSE, and are isotopically more evolved (avg. $\varepsilon Nd_{1590} = –5.9$), than granites within the central gold province (avg. $\varepsilon Nd_{1590} = –3.4$) (Hand *et al.*, 2007). Nevertheless, despite their mantle origins, it is thought that these plutons are also affected by the assimilation of country rock (Hand & Reid, 2012).

METHODS

Approach and Sampling

A total of twenty samples were collected, including five mafic enclaves, four mafic flows and twelve mafic intrusive from core samples, all belonging to the Hiltaba suite and Gawler Range Volcanics. These samples spatially range from the central Au dominated mineral system (central Gawler Craton) and eastern Gawler province, near Olympic Dam (Figure1 and Table 1). Samples with pre-existing whole-rock geochemistry, Sm-Nd isotopic data and variable Cu abundances were prioritised. Only

three enclaves, five core samples and three existing (diorite and gabbro) samples were analysed for Cu isotopes. Three enclaves and two core samples were analysed for major and trace whole-rock geochemistry, as these had no pre-existing data. The samples analysed for Cu isotopes included four mafic samples, representative of the eastern Gawler IOCG belt, and three enclaves and four core samples from the Au-rich central Gawler province (Table 1). Multiple analyses of three US Geological Survey (USGS) reference materials were included in the analysis (BCR-2, BHVO-2 and BIR-1a). The following section details the method developed for the analysis of Cu isotopes.

Table 1 Samples chosen for isotopic analysis that are closely spatially representative of the Au and IOCG mineralisation seen throughout the Gawler Craton.

Name	Drill core / field	Deposit	Unit	Province
E 2721833	Field Enclave	Unit of GRV	Upper GRV	Au
E 2721835	Field Enclave	Unit of GRV	Upper GRV	Au
E 2721815	Field Enclave	Unit of GRV	Upper GRV	Au
PDBN 321-02	Core	Barns	HS	Au
PDBN 321-04	Core	Barns	HS	Au
BLD-3	Core	Bill's Lookout	HS	Au
18-WPGTC-04	Mine wall sample	Tarcoola	HS	Au
CUR D2	Core	Curramulka	HS	IOCG
DD08WTH004	Core	White Hill	HS	IOCG
DD08WTH005	Core	White Hill	HS	IOCG
Roopena DDH2	Core	White Hill	GRV	IOCG

Petrography

Two Enclaves (R2721819 and R2721535) and three core samples (DD08WTH004, DD08WTH005 & CUR D2) were thin sectioned at Adelaide Petrographics Inc., for petrographic analysis using transmitted and reflected light microscopy. These samples were selected given the enclaves had not been previously analysed and three of the core samples appeared to have sulphide within their matrices. Only two of the four enclave

samples could be thin sectioned. Previous thin section descriptions for BLD 3 and PDBN 321-02 were gathered from Wade *et al.* (2019).

Sample Dissolution

Approximately 150 mg of all standards and samples were digested in 6 ml 2:1 mixture of HF:HNO_3 at a concentration of 15 Mol L^{-1} and 7 Mol L^{-1}, respectively, in a closed screw-top Teflon beaker then heated on a hotplate at 140 °C for 48 hours. Following this, approximately 1 mL of 15 Mol L^{-1} HNO_3 was added to the sample to prevent the formation of fluoride and to ensure all cations in the sample were converted to nitrate species. This was repeated each with each drying process. After drying, approximately 6 ml of a 2:1 mixture of HF: HNO_3 at a concentration of 15 Mol L^{-1} and 7 Mol L^{-1} was added. The beaker was then closed and the sample was heated at 140 °C for 48 hours. Following drying, 6 mL of 10 Mol L^{-1} HCl was added to each standard and sample. This solution was centrifuged at 13 200 rpm and the top portion of the samples was used for chromatography, leaving behind approximately 25 mg of sample solution to avoid adding precipitates to the chromatography column.

Ion Exchange Chromatography

Chromatography and the use of element-specific resins allows for the separation of specific elements from the rock matrix for the purposes of isotope analysis. Manual and automatic column chromatography were synchronously calibrated and standards

processed; however most of the focus of this development was on the automatic chromatographic technique.

PREPFAST MC AUTOMATIC COLUMN CHRIOMATOGRAPHY

The automated purification of Cu for isotopic analysis was performed using the prepFAST MC containing a new 1 mL Fe-Zn-Cd column (Part number CF-MC-FeZnCd-1000).

Calibration

A synthetic solution containing 1 µg/g of Cu-Zn-Fe-Co in 10M HCl was passed through a new CF-MC-FeZnCd-1000 column. Eluted fractions were collected and either analysed by Inductively Coupled Plasma Mass Spectrometry (ICP-MS) at Adelaide Microscopy for trace element content to ascertain if Cu was eluted in the correct fraction, or tested with Chlorophosphonazo (III) indicator for the presence of cations. Repeated attempts proved unsuccessful until the operating software was reinstalled by Elemental Scientific and the column was changed. All the attempts are summarised in Table 2. The source of the problem was determined by running the previously unsuccessful Sr-Ca elution, which also failed, indicating a software issue was most likely present. Two Cu separation methods were used: a calibration method where 1 ml aliquots were collected from the sample to finish, and a Co-Cu-Fe-Zn specific method where fractions were collected where these elements expected to be.

Table 2 Element separation attempts using the prepFAST MC. Adequate separation was not accomplished with both the CF-MC-FeZnCd-1000 and CF-MC-SrCa-1000 columns until the software was reinstalled and a new CF-MC-FeZnCd-1000 column was used which resulted in the copper eluting over both the matrix and copper fractions with considerable Co contamination.

Date	Sample	Column	Testing method	Result
21/03/19	1µg/g Co, Cu, Fe & Zn	CF-MC-FeZnCd-1000	ICP-MS	Fail Cu & Co eluted immediately
9/04/19	1µg/g Co, Cu, Fe & Zn	CF-MC-FeZnCd-1000	ICP-MS	Fail Cu & Co eluted immediately
29/04/19	20µg/g Cu	CF-MC-FeZnCd-1000	Chlorophosphonazo(III) indicator	Fail Cu eluted within 2 ml
14/05/19	20µg/g Cu	CF-MC-FeZnCd-1000	Chlorophosphonazo(III) indicator	Fail Cu eluted within 2 ml
27/05/19	<10µg/g Sr	CF-MC-SrCa-1000	Chlorophosphonazo(III) indicator	Fail Sr eluted within 5 ml
28/05/19	20µg/g Sr	CF-MC-SrCa-1000	Chlorophosphonazo(III) indicator	Fail Sr eluted within 5 ml
29/05/19	20µg/g Sr	CF-MC-SrCa-1000	Chlorophosphonazo(III) indicator	Fail Sr eluted within 8 ml
30/05/19	20µg/g Sr	CF-MC-SrCa-1000	Chlorophosphonazo(III) indicator	Fail Sr eluted within 6 ml
30/05/19	20µg/g Sr	CF-MC-SrCa-1000	Chlorophosphonazo(III) indicator	Non calibration. Fail No Sr in desired cut
31/05/19	100µg/g Sr	CF-MC-SrCa-1000	Chlorophosphonazo(III) indicator	Non calibration. Fail No Sr in desired cut
31/05/19	100µg/g Sr	CF-MC-SrCa-1000	Chlorophosphonazo(III) indicator	Stopped the operation
3/06/19	100µg/g Sr	CF-MC-SrCa-1000	Chlorophosphonazo(III) indicator	Fail Sr eluted within 3-7 ml
3/06/19	2M HNO_3 blank	CF-MC-SrCa-1000	Chlorophosphonazo(III) indicator	No cations
4/06/19	100µg/g Sr	CF-MC-SrCa-1000	Chlorophosphonazo(III) indicator	Fail Sr eluted within 3-7 ml
4/06/19	100µg/g Sr	CF-MC-SrCa-1000	Chlorophosphonazo(III) indicator	Fail Sr eluted within 3-7 ml
5/06/19	100µg/g Sr	CF-MC-SrCa-1000	Chlorophosphonazo(III) indicator	Sr fraction contains some Sr Matrix fraction most of Sr
11/06/19	100µg/g Sr	CF-MC-SrCa-1000	Chlorophosphonazo(III) indicator	Fail. Run to show the manufacturer the result
1/07/19	100µg/g Sr	CF-MC-SrCa-1000	Chlorophosphonazo(III) indicator	Sr run successfully in Sr cut
3/7/19	25µg/g Cu	CF-MC-FeZnCd-1000	Chlorophosphonazo(III) indicator	Cu in overlap between matrix and Cu fraction (calibration mode)
4/07/19	25µg/g Cu	CF-MC-FeZnCd-1000	Chlorophosphonazo(III) indicator	Cu in overlap between matrix and Cu fraction (calibration mode)
4/07/19	10µg/g Cu	CF-MC-FeZnCd-1000	Chlorophosphonazo(III) indicator	Cu in overlap between matrix and Cu fraction (calibration mode)
25/07/19	25 mg BIR-1a & BHVO-2	CF-MC-FeZnCd-1000	Chlorophosphonazo(III) indicator	Good separation, overlap between Cu and Co
01/08/19	25 mg BCR-2	CF-MC-FeZnCd-1000	ICP-MS	Good separation, overlap between Cu and Co
14/08/19	25µg/g Cu	CF-MC-FeZnCd-1000	Chlorophosphonazo(III) indicator	Cu in correct fraction

Standard solutions and rock standards

Variable column loads were tested with basaltic standards. MC-ICP-MS analysis indicated a 25 mg column load yielded the most accurate results. Final analysis involved a 30 mg sample load on the column with the collection of fractions between 4.5 mL to 11.5 mL to isolate Cu, while in calibration mode.

MANUAL COLUMN CHROMATOGRAPHY

A synthetic solution containing 1 µg/g of Cu-Zn-Fe-Co in 6M HCl was passed through a pre-cleaned column with anion exchange resin (Bio-Rad AG® 1-X8 200–400 mesh) with successful elemental separation (Table 3), following the method of Sossi et al. (2014). Following this, 25 mg of each standard was passed through a pre-cleaned manual column according to the procedure in table 3 with the collection of fractions between 4.5 mL to 11.5 mL to isolate Cu. These fractions were analysed on the MC-ICP-MS which proved unsuccessful, leading to this process being repeated with the collection of each 1 mL fraction for ICP-MS analysis to identify the elemental elution pattern, however not without significant overlap between Fe and Cu. For this reason the use of manual column chromatography was discontinued.

Table 3 Column chromatography procedure for a column with 1 mL AG1-X8 (200-400 mesh) resin (Sossi *et al.*, 2014)

Step	Solvent	Eluent mL	Other elements eluted
Cleaning	3 mol L^{-1} HNO3	5	
Cleaning	Milli-Q H_2O	5	
Cleaning/equilibration	6 mol L^{-1} HCl	5	
Sample load	6 mol L^{-1} HCl	0.5	Matrix
Matrix	6 mol L^{-1} HCl	4*1 (4)	Matrix
Cu	6 mol L^{-1} HCl	7*1 (7)	Co
Fe	0.5 mol L^{-1} HCl	6*0.5 (3)	Ga, Mo
Zn	3 mol L^{-1} HNO_3	5*0.5 (2.5)	Cd
Total		17	

Mass spectrometry

Copper isotopic determination was performed on the ThermoFinnigan Neptune Multi Collector (MC-ICP-MS) at CSIRO/University of Adelaide. Sample solutions were introduced by auto sampler under 'dry' plasma using a spray chamber. Samples and standards were diluted to ~300 ng mL^{-1} and measured for three blocks of 30 cycles – which is the total number measurements on a sample in one analysis – for the first two sessions and then at ~100 ng mL^{-1} for one block of 20 cycles for subsequent analysis. This was synchronous with the switch between the use of H-cones (skimmer) to the more sensitive X-cones (skimmer). Cu isotopes were analysed in low-resolution mode with ^{63}Cu in the central cup and ^{65}Cu in the H2 Faraday cup (Table 4). Copper isotopic data are reported in standard δ-notation (per mil) relative to a standard reference material NIST 976 $\delta^{65}Cu = {}^{65}Cu/{}^{63}Cu$ sample/ $^{65}Cu/^{63}Cu$ NIST 976 − 1 × 1000.

Table 4 Cup configuration used on the ThermoFinnigan Neptune MC-ICP-MS

Cup	L3	L2	L1	C	H1	H2	H3
Isotope	^{60}Ni	^{61}Ni	^{62}Ni	^{63}Cu	^{64}Ni	^{65}Cu	^{66}Ni

Data for this study was acquired on the Neptune over four analytical sessions. Regular analysis of a nickel spike solution (^{61}Ni/^{60}Ni) and sample standard bracketing allowed for instrumental drift and mass fractionation to be monitored and automatically corrected for in the first two sessions. Analysis of Ni-spiked BIR-1a, BHVO-2 and BCR-2 revealed higher than reported δ^{65}Cu values. In comparison, unspiked standards produced lower δ^{65}Cu values, closer to their reported values. It is suspected that the Ni-spikes may have been effected by the presence of Co within the Cu cuts. The possible production of Co + H during analysis would result in higher measured values of ^{60}Ni than is present in the sample (i.e. polyatomic interference). This could serve to explain why the calibration for Ni-spiked standard solutions consistently produced lower δ^{65}Cu values than reported values. Following this, solutions in subsequent sessions were not spiked with Ni. This minimised any possible interference and produced more accurate δ^{65}Cu values for USGS standards. Instrumental drift and mass fractionation was monitored in unspiked runs using standard sample bracketing alone.

BCR-2 was not used in subsequent analyses, due to its high concentration of Fe over Cu (Fe/Cu ca. 4900) which often resulted in spurious results. USGS standards BHVO-2 and BIR-1a, which have appreciably lower Fe/Cu ratios of ca. 650, were used instead. The final session concluded with sample analysis and NIST-976 that had been passed through the column, testing for blank influence and resin induced fractionation (Table 5).

Table 5 Total analyses by MC-ICP-MS performed in this study

Sample	Run	Separation method	Sample Load	Ni-Spike	Blocks/cycles
BIR-1a	1	Manual	25 mg	Yes	3/30
BHVO-2	1	Manual	25 mg	Yes	3/30
BCR-2	1	Manual	25 mg	Yes	3/30
BIR -1a	2	PF	25 mg	No	3/30
BHVO-2	2	PF	25 mg	No	3/30
BIR -1a	2	PF	25 mg	Yes	3/30
BHVO-2	2	PF	25 mg	Yes	3/30
BIR -1a	2	Manual	25 mg	Yes	3/30
BHVO-2	2	Manual	25 mg	Yes	3/30
BIR -1a	2	Manual	25 mg	No	3/30
BHVO-2	2	Manual	25 mg	No	3/30
BIR-1a	3	PF	5 mg	No	1/20
BIR-1a	3	PF	25 mg	No	1/20
BHVO-2	3	PF	5 mg	No	1/20
BHVO-2	3	PF	10 mg	No	1/20
BHVO-2	3	PF	25 mg	No	1/20
BIR-1a	4	PF	50 mg	No	1/20
BHVO-2	4	PF	50 mg	No	1/20
NIST 976	4	PF	3 μg/g	No	1/20
E2721833	4	PF	30 mg	No	1/20
E2721815	4	PF	30 mg	No	1/20
E2721835	4	PF	30 mg	No	1/20
BLD-3	4	PF	30 mg	No	1/20
PDBN 321-02	4	PF	30 mg	No	1/20
PDBN 321-04	4	PF	30 mg	No	1/20
18-WPGTC-04	4	PF	30 mg	No	1/20
DDH2	4	PF	30 mg	No	1/20
CUR D2	4	PF	30 mg	No	1/20
DD08WTH004	4	PF	30 mg	No	1/20
DD08WTH005	4	PF	30 mg	No	1/20

Geochemistry

Five samples – two gabbros (DD08WTH005, DD08WTH004) and three mafic enclaves (E2721815, E2721833, and E2721835) – were analysed for whole-rock major and trace element geochemistry by ICP-MS at Adelaide Microscopy. The remaining samples all

had pre-existing whole rock geochemistry. Sample powders of 18-WPGTC-04, PDBN 321-04 and PDBN 321-02 powders where provided by Justin Payne (University of South Australia), while samples including BLD-3, CUR D2 and Roopena DDH2 were sampled from the same region and previously analysed for their geochemistry by Claire Wade (The University of Adelaide/ Geological Survey of South Australia).

OBSERVATIONS AND RESULTS

Petrography

Mafics from the IOCG province (DD08WTH004, DD08WTH005, CUR D2) are phaneritic and medium grained gabbro, containing abundant plagioclase, clinopyroxene, orthopyroxene, minor biotite, disseminated sulfides and no ground mass. All samples contain trace amounts of chalcopyrite (<1%) and pyrite (~3%), however the abundance and grain size of these minerals is lower in CUR D2 (<1% and ~2% respectively). All sulfides overprint orthopyroxene and chalcopyrite appears to overprint pyrite. No alteration is seen within the samples indicating the sulfide is likely magmatic.

E2721835 is a glomerophyric mafic enclave with phenocrysts of euhedral plagioclase, amphibole and possibly poikiloblastic potassium feldspar, set in a fine-grained matrix consisting of an unidentifyable red mass. Trace amounts of ilmenite (~1%) and titanite (<1%) are present. No sulfides are present within the samples. No alteration is seen.

E2721819 is a glomerophyric mafic enclave containing heterogenetic amalgamations of anhedral quartz, muscovite as a finer grained matrix as well as euhedral opaque minerals. Phenocrysts of amphibole and potentially plagioclase are also present. This sample did not undergo isotopic analysis as is believed to be a clast of pre-existing crustal material and not a magmatic enclave (Figure 3g).

Petrographic analysis of central Gawler Craton samples BLD 3 and PDBN 321-02 by Wade *et al*. (2019), indicated a lack of sulfides and alteration within these samples.

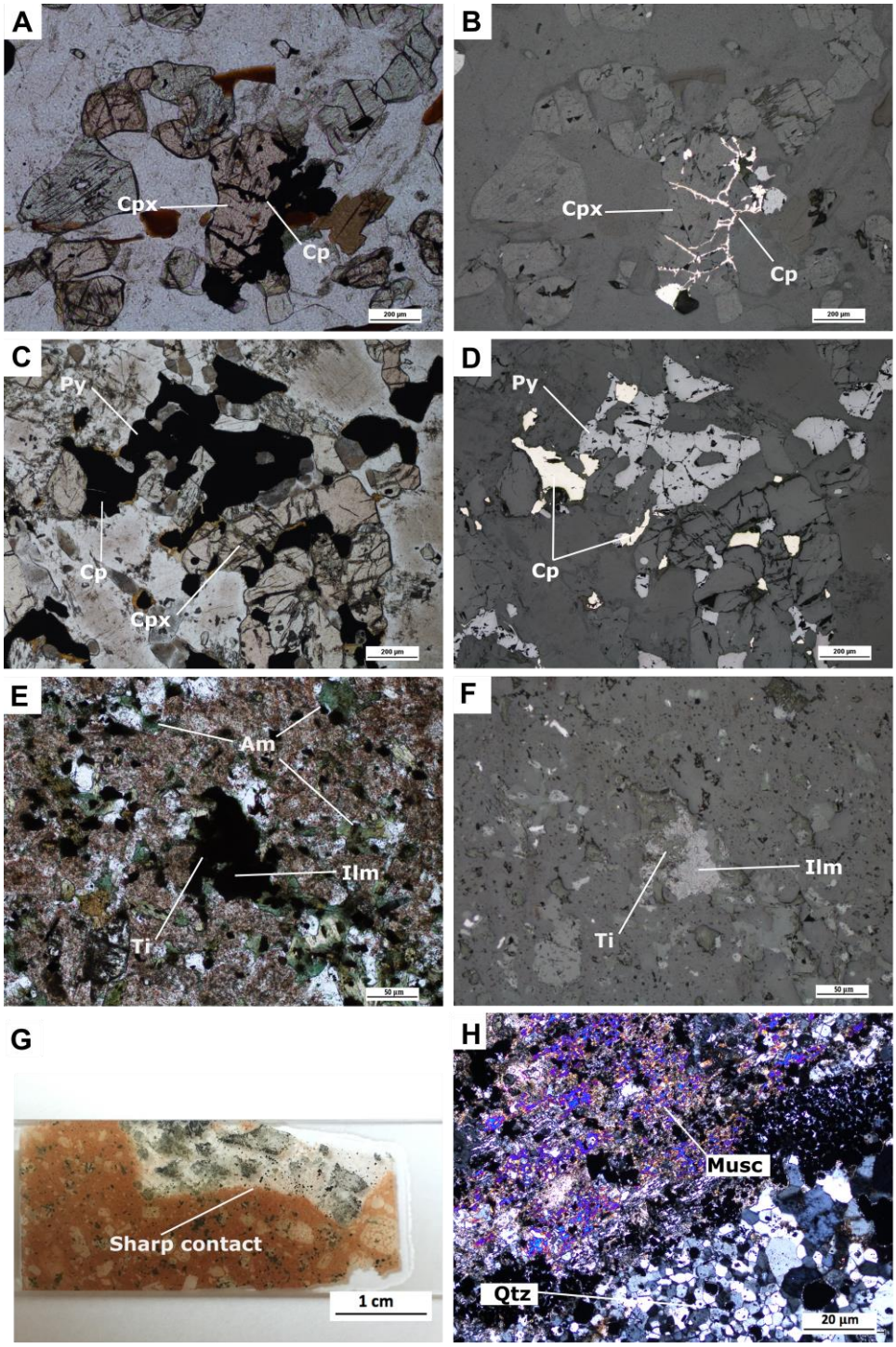

Figure 3 Petrographic analysis of mafic samples of the Hiltaba Suite and Gawler Range Volcanics, a) Opaques overprinting orthopyroxene, drill hole CUR D2, b) reflected light showing chalcopyrite infill, drill hole CUR D2, c) opaque minerals seen in close relationship with orthopyroxene, drill hole DD08WTH004 which also represents textures seen in DD08WTH005, d) reflected light showing chalcopyrite overprinting pyrite within in the same mineral assemblage, e) & f) titanite rim with ilmenite with a lack of sulfides present in E2721835, g) thin section showing sharp angular contact between clast and host rock in E2721819, f) abundant muscovite and quartz indicating the sample E2721819 is a clast rather than an enclave.

Geochemistry

The following reports the whole-rock geochemistry of all samples used for Cu isotope analysis. Mafic samples from the Hiltaba Suite display variable major element compositions with Al_2O_3 ranging between 8.9 and 18.4 wt%, Fe_2O_3 between 8.5 and 25.5 wt%, K_2O between 0.3 and 4.4 wt%, MgO between 2.0 and 5.8 wt% and CaO ranging between 2.0 and 10.5 wt% (Figure 4).

Mafic enclaves are distinguished from central and eastern Gawler Craton samples (C G.C., E G.C.) by their lower MgO contents. Mafic enclaves also have lower CaO and higher K_2O, Na_2O and TiO_2. Samples from the IOCG (E G.C.) and C G.C. provinces are more mafic with a higher MgO contents and cannot be distinguished from one another using major element compositions alone, with the exception of Na_2O, which is more concentrated in the IOCG province (E G.C.) samples. Coherent trends are formed between Na_2O and CaO against MgO in all three sample groups (Figure 5).

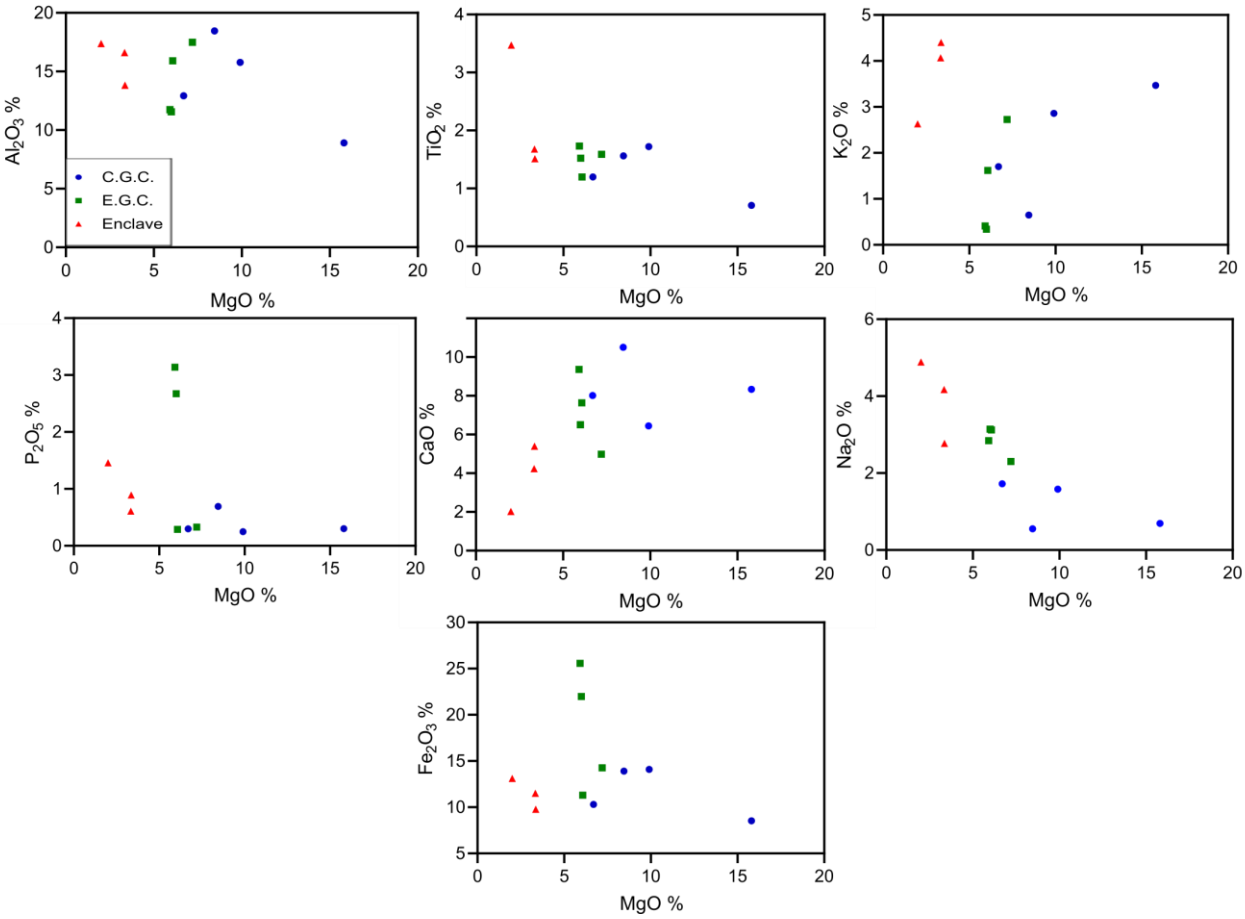

Figure 4 Major element composition vs MgO wt. % for mafic samples analysed within the study, from central Gawler Craton (C.G.C), eastern Gawler Craton (E.G.G) and Enclaves from the C.G.C.

All of the samples analysed in this study can be classified as basalts to basaltic andesites according to the Nb/Y and Zr/Ti trace element classification by Pearce (1996). According to Pearce (1996) the enclaves are more andesitic in composition (figure 5). This is in agreement with their major element composition – in particular lower MgO contents –which otherwise suggests that the magmas which formed the enclaves were more felsic than those from the Central and Eastern Gawler Craton (CGC, EGC).

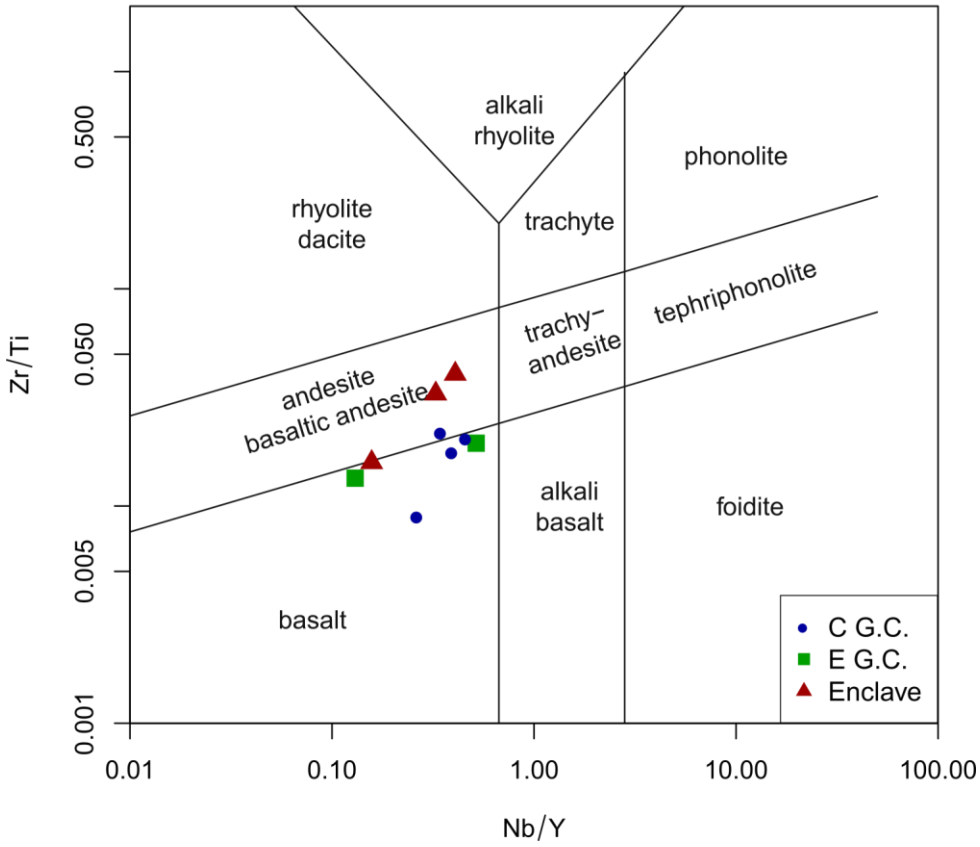

Figure 5 Nb/Y – Zr/Ti plot indicating the enclaves are more felsic than samples from C G.C and E G.C (modified by Pearce 1996).

The trace element abundances between each of the sample groups are highly variable. The mafic enclaves are characterised by their significantly higher Ba, REE (La-Lu), Hf, Mo, Nb, Th and U contents.

The primitive mantle normalised (PMN) spidergram (normalising values from Sun and McDonough (1989)) can be found on figure 6. Incompatible elements on the left, trending to compatible elements on the right. All the samples appear to follow a negatively sloping trend with enrichments in light REE (LREE) relative to heavy REE (HREE) (La/Yb_N = 2.1 −27.6). Samples share depletions in Nb, Sr and enrichments in

Cs, Pb, U and P. The Eastern Gawler Craton samples appear most variable in composition with strong depletions in Zr and Nb and enrichment in P in the samples from White Hill (DD08WTH004 & DD08WTH005). The mafic enclaves are generally more enriched than other sample groups. The Central Gawler Craton samples follow a similar trend, however show strong enrichment in Pb.

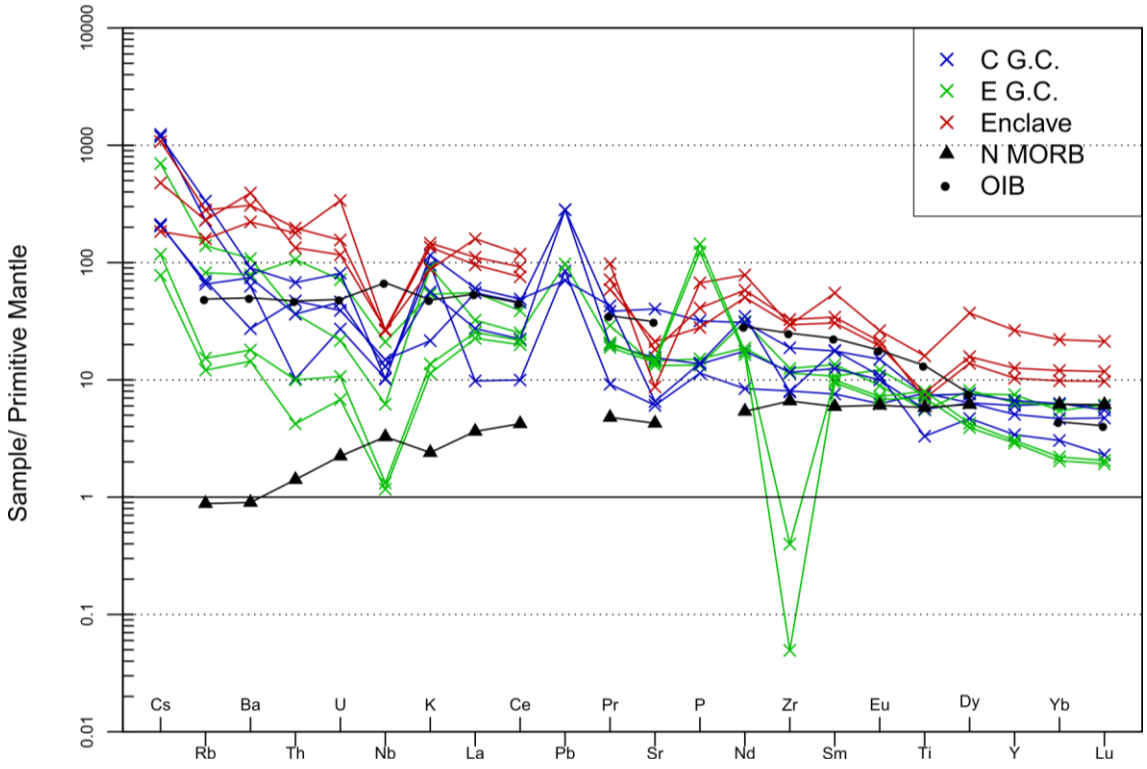

Figure 6 Primitive mantle-normalised trace element diagram for the sample suite analysed in this study.

A positive correlation Cu and Sc, however no other elemental correlation can be seen with Cu (Figure 7).

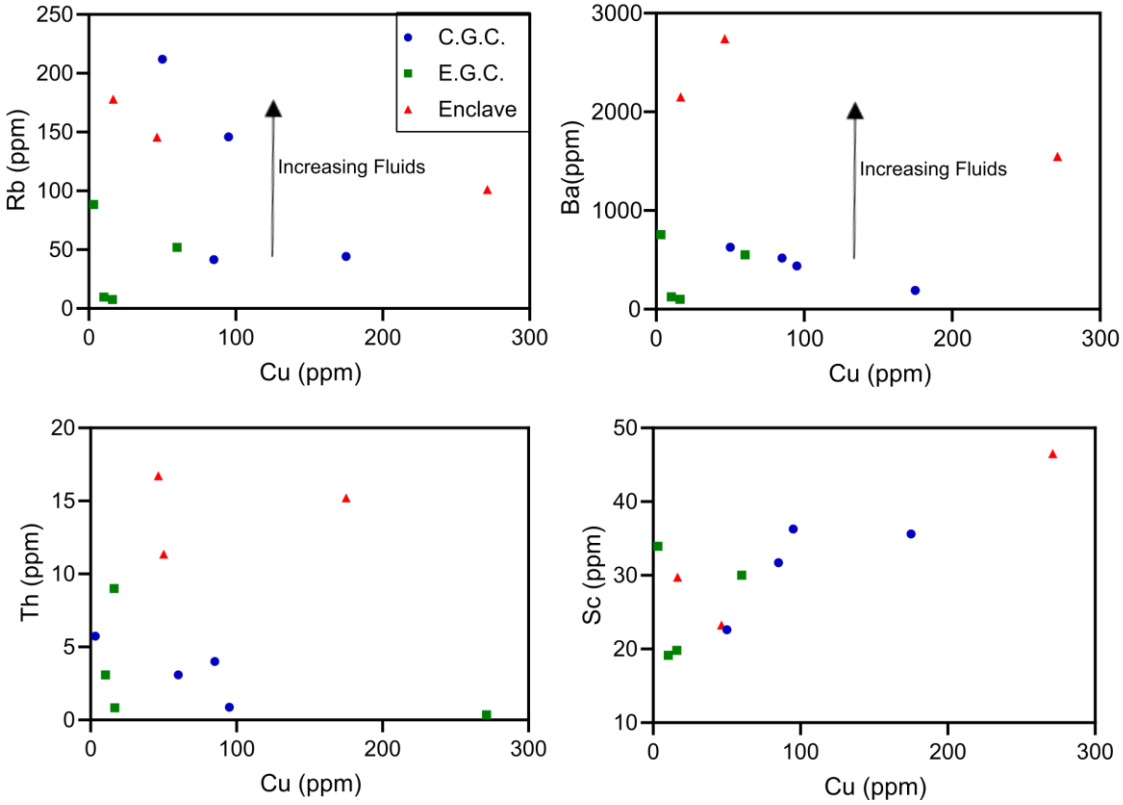

Figure 7 Relationships between elemental abundance and Cu abundance within the sample set, indicating enclaves are fluid rich (high Rb and Ba) and contain high Th values, possibly indicating crustal assimilation.

Table 6 Whole-rock geochemical and Cu isotope composition of mafic samples analysed in this study. Mg number was not calculated as whole-rock geochemistry was gathered by ICP-MS.

Sample	Bills Lookout	18WPGTC-04	Barns	Barns	Enclave 1	Enclave 2	Enlcave 3	DD08WTH004	DD08WTH005	Curramulka	Roopena DDH
Drill Hole	BLD 3	out crop	PDBN321-02	PDBN321-04	out crop	out crop	out crop	DD08WTH004	DD08WTH005	CURD2	Roopena DDH 2
Location	Bills Lookout	Tarcoola	Barns	Barns	C.G.C	C.G.C	C.G.C	White Hill	White Hill	Curramulka	GRV out crop
Province	C.G.C	C.G.C	C.G.C	C.G.C	C.G.C	C.G.C	C.G.C	E.G.C	E.G.C	E.G.C	E.G.C
Age (Ma)	1590	1590	1590	1590	1590	1590	1590	1590	1590	1590	1590
Depth from (m	927.2	Unavailable	Unavailable	Unavailable	N/A	N/A	N/A	315.7	317.2		71.2
Depth to (m)	927.3							315.8	317.3		71.3
Source	C. Wade	J. Payne	J. Payne	J. Payne	This study	This study	This study	This study	This study	C. Wade	C. Wade
Lithology	Diorite	Diorite	Aphanitic dyke	Aphanitic dyke	Basaltic enclav	Basaltic enclav	Basaltic enclav	Basalt	Basalt	Norite	basalt
Major elements (wt%)											
SiO2	42.5	48.6	50.4	40.0						51.9	45.0
Al2O3	15.8	12.9	8.9	18.5	13.8	17.4	16.6	11.6	11.7	15.9	17.5
CaO	6.4	8.0	8.3	10.5	5.4	2.0	4.2	6.5	9.4	7.63	5.0
Fe2O3	14.1	10.3	8.5	13.9	9.8	13.1	11.5	22.0	25.6	11.3	14.3
K2O	2.9	1.7	3.5	0.6	4.4	2.6	4.1	0.3	0.4	1.62	2.7
MgO	9.9	6.7	15.8	8.5	3.4	2.0	3.3	6.0	5.9	6.07	7.2
Na2O	1.6	1.7	0.7	0.6	2.8	4.9	4.2	3.1	2.8	3.12	2.3
P2O5	0.2	0.3	0.3	0.7	0.9	1.5	0.6	2.7	3.1	0.29	0.3
SO3	0.1	0.4	0.0	0.1							
TiO2	1.7	1.2	0.7	1.6	1.5	3.5	1.7	1.5	1.7	1.2	1.6
MnO	0.2	0.2	0.2	0.3	0.2	0.4	0.3	0.2	0.2	0.16	0.2
BaO	0.0	0.1	0.1	0.0	0.3	0.2	0.2	0.0	0.0		
Cl	0.1	0.0	0.0	0.0							
LOI	4.5	7.8	2.0	5.0						0.95	
Trace and rare earth elements (ppm)											
Ga	18.1	17.2	14.2	30.2	23.7	38.1	28.2	20.5	21.4	20	27.2
Cr	356.0	412.0	1510.0	189.0	39.6	18.6	25.9	41.3	31.5	80	91.6
Ni	215.0	90.0	625.0	90.0	24.6	21.0	15.0	8.2	8.6	39	61.1
Co	54.9	43.9	64.7	54.9	38.3	101.3	87.4	80.0	105.1	27	46.8
Sc	36.3	31.7	22.6	35.6	23.2	46.5	29.7	19.8	19.2	30	33.9
Ti	10000.0	7310.0	4300.0	9590.0	9030	20800	10100	9110	10400		
V	311.0	247.0	113.0	205.0	155	309	157	274	306	220	204
Cu	95.0	85.0	50.0	175.0	46.4	271.3	16.6	16.2	10.2	60	3.3
Zn	165.0	200.0	105.0	175.0	147.1	469.6	202.3	89.2	131.9	39	115
Y	27.5	23.1	15.5	30.2	47.0	120.2	57.3	13.2	13.9	29	34.0
Rb	146.0	41.6	212.0	44.3	146.0	101.0	178.0	7.7	9.7	52	88.4
Sr	128	326	138	848	382	184	447	296	315	280	305
Cs	9.8	1.7	9.4	1.6	3.8	1.5	8.5	0.6	0.9	<3	5.5
Ba	439.0	519.0	628.0	191.0	2741	1550	2150	101	126	550	755
Th	0.9	3.1	5.7	4.0	11.4	15.2	16.7	0.4	0.8	9.0	3.1
U	0.6	1.0	1.7	0.8	2.4	7.1	3.3	0.1	0.2	1.5	0.5
Pb	6.0	20.0	5.0	20.0						<3	6.9
Zr	90.0	130.0	88.5	210.0	366.0	330.5	330.8	0.6	4.5	140	128
U	0.6	1.0	1.7	0.8	2.4	7.1	3.3	0.1	0.2	1.5	0.5
Zr	90.0	130.0	88.5	210.0	366.0	330.5	330.8	0.6	4.5	140	128
Hf	2.5	3.6	2.7	5.2	9.7	9.5	9.4	0.0	0.1	6.0	
Nb	7.4	9.2	7.2	10.6	19.1	18.9	18.7	0.8	0.9	15	4.4
Ta	0.5	0.5	0.5	0.4	1.8	1.5	1.5	0.3	0.3	2.0	0.4
La	6.7	18.8	41.4	37.9	76.2	109.5	65.7	15.5	17.4	38	22.2
Ce	17.7	39.5	86.8	81.3	162.9	209.2	134.2	35.4	38.5	69	44.6
Pr	2.5	5.5	11.8	10.6	19.7	27.0	16.3	5.2	5.5	8.0	5.7
Nd	11.4	23.8	47.1	41.7	78.6	106.2	68.3	22.2	23.6	42.5	25.3
Sm	3.4	5.5	7.9	7.8	15.2	24.4	13.6	4.2	4.4	6.0	4.8
Eu	1.1	1.7	1.8	2.5	3.6	4.4	3.3	1.1	1.2	1.5	2.0
Gd	4.4	5.4	5.3	6.6	13.1	26.3	13.1	4.0	4.3	6.0	6.4
Tb	0.8	0.9	0.7	1.0	57.1	233.9	34.6	0.9	1.5	1.0	0.9
Dy	4.7	4.7	3.5	5.6	10.2	27.4	11.6	2.9	3.1	6	5.6
Ho	1.1	1.0	0.7	1.2	2.0	5.3	2.3	0.5	0.6	1.0	1.0
Er	3.2	2.4	1.6	3.1	5.6	14.2	6.6	1.4	1.5	4	3.2
Tm	0.5	0.4	0.3	0.5	0.8	1.8	0.9	0.2	0.2		0.4
Yb	3.1	2.3	1.5	3.1	4.8	10.9	5.9	1.0	1.1	3.0	2.7
Lu	0.4	0.4	0.2	0.4	0.7	1.6	0.9	0.1	0.2		0.5
εNd and δ65 Cu isotopic compositions for mafic Hiltaba suite samples											
εNd	-5.49	1.95	-0.76	-1.96						-3.36	2.46
δ65 Cu	0.397	0.186	0.084	0.434	-0.053	-0.199	-0.897	1.422	1.057	0.178	0.69
2SD	0.011	0.379	0.23	0.032	0.023	0.018	0.006	0.077	0.111	0.017	0.024

Chromatographic separation

The initial separation of 1 µg/g of Cu-Zn-Fe-Co via the column chromatography proved unsuccessful for the automatic prepFAST MC system, with Co, Cu and Fe all eluting, at least partially, in the matrix fraction (Figure 8).

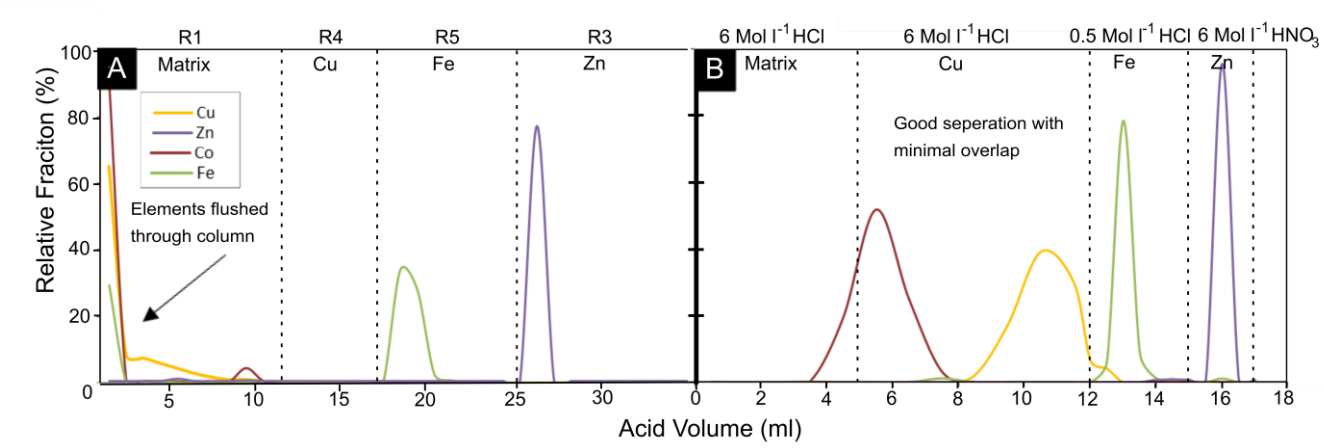

Figure 8 Elution curves for Cu, Co, Fe and Zn from 1 µg/g of Cu-Zn-Fe-Co solution in (A) CF-MC-FeZnCd-1000 column in the prepFAST MC system and (B) AG1-X8 (200–400 mesh) in a 0.4 x 8 cm aspect ratio column. Inefficient separation is visible using automatic separation compared to manual. (R1= 10 M HCl + 0.01% H_2O_2, R2 = 10 M HCl, R3 = H_2O, R4 = 5 M HCl R4 =5 HCl+ 0.01% H_2O_2, R5 = 1M HCl).

Separation using basaltic standards (BCR-2) was unsuccessful relative to literature, for both the manual and automatic columns. The manual column released Cu late within the elution sequence, causing a complete overlap between Cu and Fe. The BCR-2 processed by automatic chromatography resulted in substantial overlap between Cu and Co, however separation with other matrix elements was successful (Figure 9).

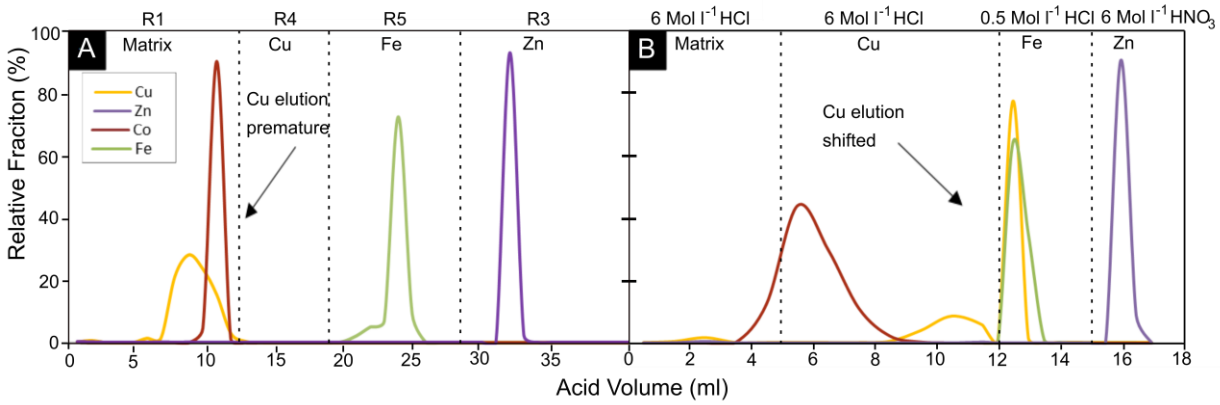

Figure 9 Elution curves for Cu, Co, Fe and Zn from BCR-2 in (A) CF-MC-FeZnCd-1000 column in the prepFAST MC system and (B) AG1-X8 (200–400 mesh) in a 0.4 x 8 cm aspect ratio column. Inefficient separation is visible using automatic separation compared to manual. (R1= 10 M HCl + 0.01% H_2O_2, R2 = 10 M HCl, R3 = H_2O, R4 = 5 M HCl R4 =5 HCl+ 0.01% H_2O_2, R5 = 1M HCl).

Isotopic analysis

SPIKING

Ni spike corrections using $^{60}Ni/^{61}Ni$ gave results that were more inaccurate than corrections using only bracketing standards for samples BCR-2, BIR-1a and BHVO-2 on run two on the MC-ICP-MS. Concentrations of Co over Cu appeared high within the purified BHVO-2, BCR-2 (Co/Cu ca. 0.2 and 3.4 respectively) which appeared to create an interference potentially with ^{60}Ni.

DRIFTING

Measurement of standard solutions over three blocks across thirty cycles revealed some instrumental drift. Consequently, the total cycles were decreased to one block of twenty cycles, which appeared to minimize instrumental drift during data acquisition (Figure 10).

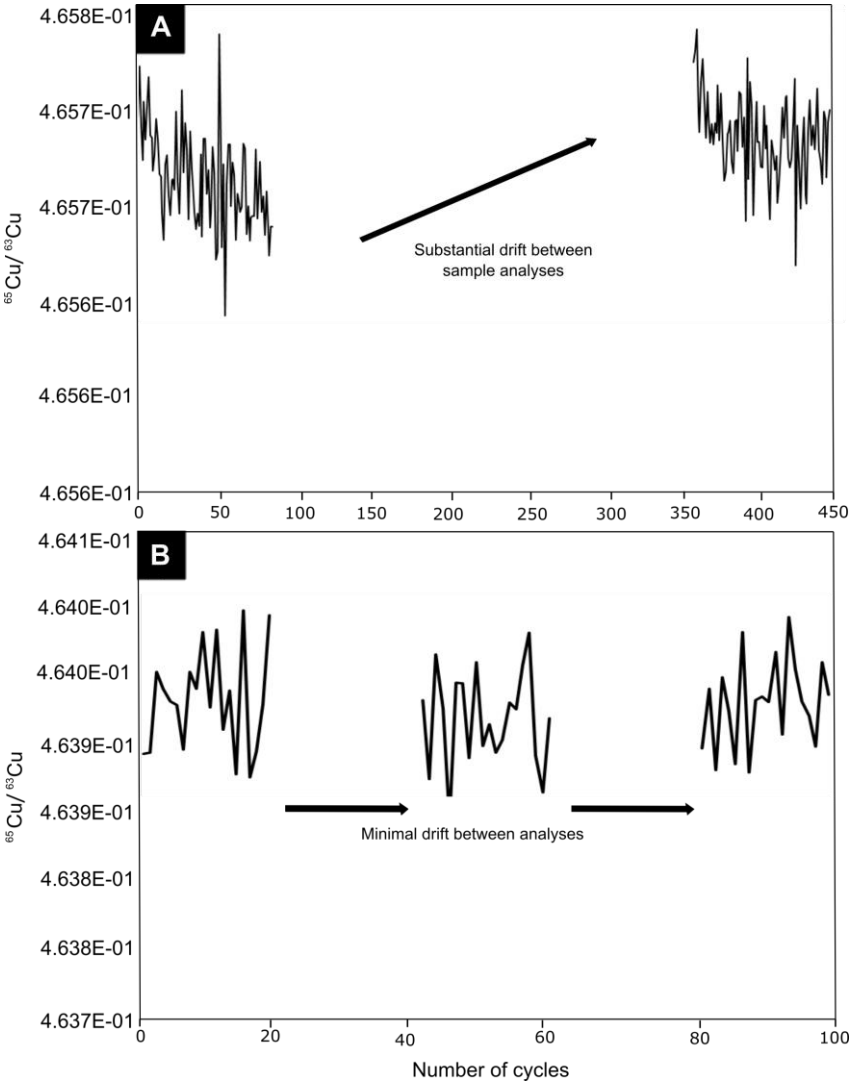

Figure 10 Measurement of $^{65}Cu/^{63}Cu$ in NIST 976 standard during sample standard bracketing between samples and blanks, which are not seen, at (a) three blocks of 30 cycles and (b) one block of 20 cycles.

ISOTOPIC ANALYSIS

A total of eleven samples were analysed for their Cu isotopes of which data from eight samples was deemed accurate and reproducible. Of these eight samples three were from the IOCG province (eastern Gawler Craton) and five were from the Au-only province (central Gawler Craton). Values from the manual chromatographic separation were discarded, along with values with two standard deviations (2 S.D) > ~ 0.3, only if other runs proved more precise. All remaining results were checked for their quality by analysing their raw count data against time to identify any irregularities or instrumental drift which otherwise could not be readily identified in the standard deviation. A weighted mean was calculated for the samples with multiple results that were deemed of good quality. With the use of sample standard bracketing (NIST-976) and a decrease to one block of twenty cycles, the most accurate δ^{65}Cu value obtained for a USGS reference standard was BIR-1 with a value of 0.115‰ and a reproducibility of ±0.010‰ (n=2), in comparison to literature values of 0.00‰ and a reproducibility of ±0.03‰ (n=2) (Sossi *et al.*, 2014). A weighted mean of 0.123‰ with a reproducibility of ±0.013‰ (n=4) was obtained with final values for BIR-1a. Samples analysed in this study show variable δ^{65} Cu values between –1.085 and +1.422‰ (Figure 11). The procedural blank was in the order of 0.02 ng mL^{-1} relative to the amount processed through the columns (Cu ≈ 100 – 8000 ng mL^{-1}). Isotopic analysis of NIST-976 processed through the automatic column yielded a δ^{65} Cu result of – 0.036‰ and a reproducibility of ±0.026‰ (n=2) (Table 7).

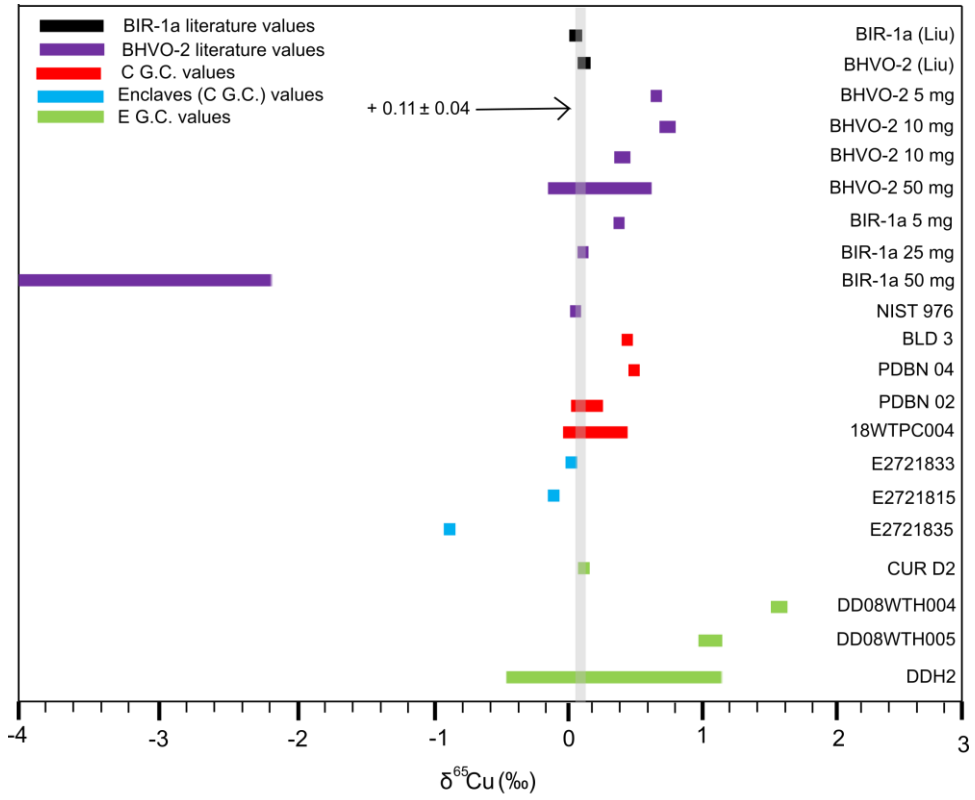

Figure 11 δ^{65} Cu ranges of samples analysed within this study, including literature δ^{65} Cu values for BIR-1a and BHVO-2 (Liu *et al.*, 2014).

Table 7 Cu isotopic composition of mafic standards and samples analysed in this study.

Sample	Sample load on column	Session	Seperation Technique	δ^{65} Cu Unspiked (‰)	δ^{65} Cu Ni Spiked (‰)	2SD	*n*	Comments
BCR-2	25 mg	1	Manual	2.002	4.312		1	Ni correction appears to worsen the results
	25 mg	2	Manual	1.39			1	
	25 mg	2	Manual	−1.32			1	
BHVO-2	25 mg	1	Manual	1.719	0.767		1	Spiked value ignored
	25 mg	2	PF	0.479			1	
	25 mg	2	Manual	0.525			1	
	25 mg	2	PF	0.273	−6.120		1	Spiked value ignored
	25 mg	2	Manual	0.409	0.003		1	Spiked value ignored
	5 mg	3	PF	0.559		0.030	2	Ni Spiked
	10 mg	3	PF	0.706		0.051	2	Ni Spiked
	25 mg	3	PF	0.334		0.048	2	
	50 mg	3	PF	0.084		0.416	2	
Average (n=9)				0.565				
BIR-1a	25 mg	1	Manual	1.070	2.728	1.272	2	Ni correction appears to worsen the results
	25 mg	2	PF	0.159			1	
	25 mg	2	Manual	0.206			1	No Ni spike, drifting as well overnight as not enough NIST standards run
	25 mg	2	PF	0.132	-3.980		1	Spiked value ignored
	25 mg	2	Manual	0.133	0.237		1	Spiked value ignored
	5 mg	3	PF	0.311			1	
	25 mg	3	PF	0.115		0.010	2	
	50 mg	4	PF	−3.247		0.895	2	Discarded
Weighted mean (n=4)				0.123		0.013		Weighted mean not including discarded values
NIST 976	3 µg/g	4	PF	−0.036		0.026	2	Close to theoretical value
E2721833	30 mg	4	PF	−0.053		0.023	2	Good
E2721815	30 mg	4	PF	−0.199		0.018	2	Good
E2721835	30 mg	4	PF	−1.085		0.076	2	Good
	30 mg	4	PF	−0.723		0.076	2	Discard via cycle
	30 mg	4	PF	−0.237		0.154	2	Discard via cycle
	30 mg	4	PF	−0.896		0.004	2	1st and last best- weighted mean of both
BLD-3	30 mg	4	PF	0.397		0.011	2	Good
	30 mg	4	PF	0.083		0.170	2	Discard
PDBN 321-02	30 mg	4	PF	0.084		0.230	2	Caution
PDBN 321-04	30 mg	4	PF	0.434		0.032	2	Good
18WTPC04	30 mg	4	PF	0.186		0.379	2	Caution
DDH2	30 mg	4	PF	0.384		0.843	2	Discard
	30 mg	4	PF	0.690		0.024	2	Good
CUR D2	30 mg	4	PF	0.178		0.017	2	Good
DD08WTH004	30 mg	4	PF	1.422		0.077	2	Good
DD08WTH005	30 mg	4	PF	1.057		0.111	2	Keep

ICPMS analysis on the purified rock samples indicated low levels of contamination of throughout most of the samples. Nevertheless, samples including BIR (50 mg), CUR D2, DD08WTH005, DD08WTH004 and E2721833 contain substantial amounts matrix Ti, Na, Mg and Co after purification by column chromatography. There appears to be a correlation between highly fractionated δ^{65} Cu values matrix element abundance (Figure 15).

DISCUSSION

Analytical methods

The following will firstly discuss the method developed for the purification and analysis of Cu isotopes in bulk rock. Secondly the bulk rock Cu isotopes of mafic rocks from the Gawler Craton will be presented and the application of this technique to ore-forming processes will be discussed.

NI SPIKIKNG PRIOR TO δ^{65} CU MEASUREMENT LEADS TO ANOMALOUS AND ERRATIC RESULTS

The failure of the Ni spiking using ^{60}Ni and ^{61}Ni may possibly be attributed to the presence of double charged ions of Sn and Te. Analysis of the cuts by ICP-MS after session two did not test for these elements, however analysis of cuts from session four indicated minimal abundances, with every sample below detection limit (Gall, Williams, Siebert, & Halliday, 2012). Other interferences may originate from the

formation of polyatmomic molecules including $^{44}Ca^{16}O+$ and $^{24}Mg^{36}Ar$, which affect ^{60}Ni, and $^{25}Mg^{36}Ar$ which affect ^{61}Ni, however the natural abundances of these molecules is very low and is unlikely the only cause of variation in results. In conclusion the Ni spiking method was ineffective and lead to erratic results; more consistent results were achieved using sample-standard bracketing methods.

INCOMPLETE RECOVERY OF CU LEADS TO ANOMALOUS δ^{65} CU VALUES

The first isotopic analytical session yielded the most inaccurate results for USGS standards BCR-2, BIR-1a and BHVO-2, yielding $\delta^{65}Cu$ values of +2.002‰, +1.719‰ and +1.070‰, respectively. This session used sample standard bracketing and Ni-spiking. This high degree of variability compared to literature values (0.00‰ for BIR-1, 0.15‰ for BHVO-2 and 0.22‰ for BCR-2) (Sossi *et al.*, 2014), is likely attributed to the incomplete recovery of Cu using manual column chromatography. An elution curve of BCR-2 passed through the manual column indicated that Cu was released late and there was substantial overlap of Cu with Fe. This late release resulted in incomplete recovery as samples collected were from fractions 4.5-11.5 ml (Figure 9). Many studies have demonstrated the influence of incomplete recovery on δ^{65} Cu values (Borrok, Wanty, Ridley, Wolf, Lamothe *et al.*, 2007; S.-A. Liu, Li, Li, Teng, Ke *et al.*, 2013; Sossi *et al.*, 2014), whereby interactions between the resin and metal complex result in resin induced fractionation in the order of as much as 5‰ for copper. Furthermore, fractionation causes the heavier Cu isotopes to be eluted first followed by the lighter isotopes (S.-A. Liu *et al.*, 2013; Sossi *et al.*, 2014). This may lead to sampling bias. It is

therefore important to ensure the sampling method is consistent between samples and that the eluted sample is representative of the bulk rock.

NIST-976 standard, processed through the PrepFAST automatic column, returned a δ^{65}Cu value of –0.036 ± 0.026‰, suggesting complete recovery of Cu within the standard. Nevertheless, this cannot irrefutably confirm the complete recovery of Cu from other samples given the variability in matrix elements may affect the resin (Sossi *et al.*, 2014). Final Cu concentrations within the sample set analysed ranged from 100.2 to 162.6 ng mL^{-1}, which could raise concerns of incomplete recovery, even though theoretical recovery is over 100% for both. Nonetheless, this variability is likely due to human error during dilution. In fact the Cu concentration of NIST-976 (87.8 ng mL^{-1}) has an accurate isotopic value (δ65Cu= –0.036 ± 0.026‰), indicating human error during dilution is the likely cause rather than incomplete recovery (Figure 12).

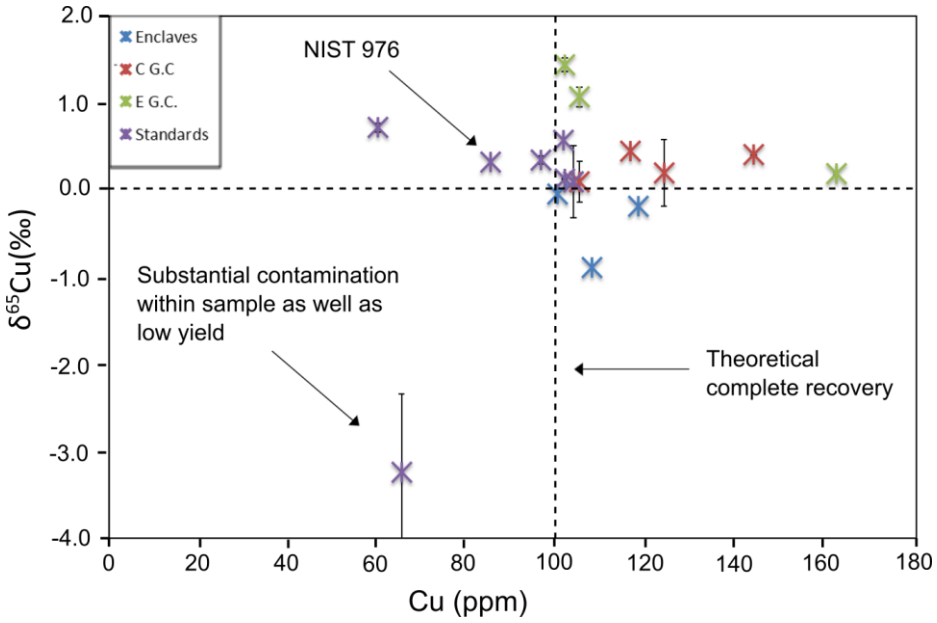

Figure 12 δ^{65}Cu (‰) vs Cu recovery giving an indication of relative recovery and its effect on Cu fractionation. The data shows a lack of trend with Cu recovery and δ^{65}Cu values indicating complete recovery during sample purification.

CORRELATING COLUMN LOAD AND MATRIX ELEMENTS

Incomplete elution of the matrix led to high concentration of major ions (Na, Mg, Ti, Co, Fe) in the purified Cu cuts. The amount of sample loaded on the column (column load) only appeared to affect Co and Ti abundances. A direct, inverse relationship between column load and Co and Ti concentrations is observed (Figure 13). Titanium is generally a prevalent contaminant within BHVO-1a, likely due to its higher elemental abundance within the sample. The cause of this inverse relationship with column load is unknown, and cannot be attributed to a blank effect, as the NIST-976 was free of Ti. The abundance of Mg appeared to be consistent throughout the load range, however a 50 mg column load of BIR-1a showed Mg/Cu values of ~5, This was the only standard with elevated Na/Cu levels (~ 22) with other standards ranging between 0.01-0.03. A 50 mg column load of BHVO did not contain substantial matrix elements, with the most notable impurity being Co at 0.4 Co/Cu. This elevated concentration in BIR-1a is possibly due to overloading of the resin (the type of which is unknown) in the CF-MC-FeZnCd-1000 column as it has a fixed number of anionic sites available in addition to BIR-1a containing higher concentrations of major ions (Na, Mg, Fe, Al). Nonetheless, a sample overloaded would usually result in elements flushed through within the first fraction (Sossi *et al.*, 2014), which is not seen, as the Cu cut was collected between 5-15 mL. In summary, there is a relationship between uneluted matrix elements (especially Ti) and column load that may affect the measurement of the true δ^{65} Cu value. This is corrected for in a following section.

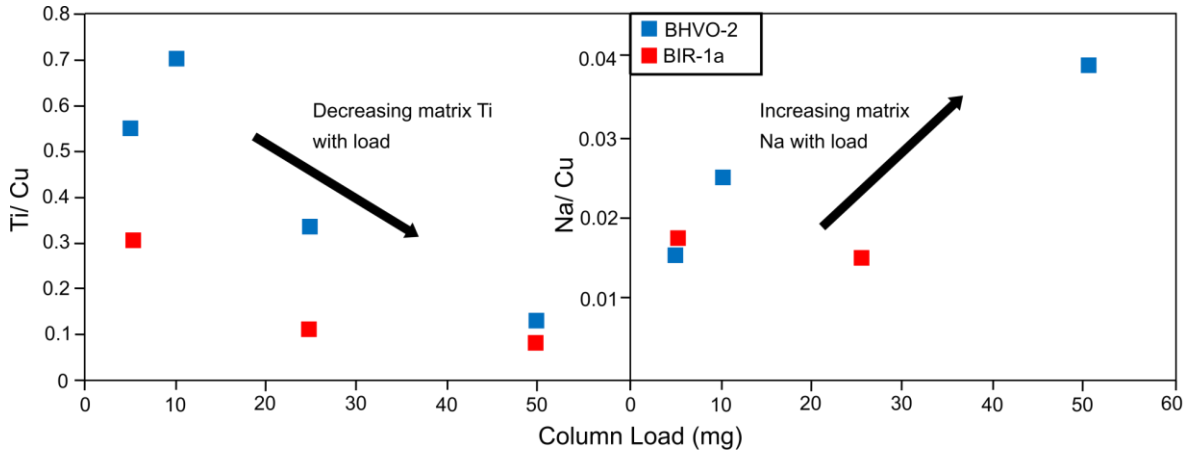

Figure 13 Sample load relative to matrix Ti and Na after chromatographic separation.

Table 8 Elemental abundance ratio relative to Cu, in purified Cu cuts.

Sample	Na/Cu	Mg/Cu	Co/Cu	Ti/Cu	Fe/Cu
DDO8WTH005	0.28	0.71	10.80	1.54	2.54
DDO8WTH004	0.08	0.44	5.12	0.99	0.12
CUR D2	0.02	1.25	0.79	0.19	0.03
E2721835	0.04	0.05	0.83	0.36	0.03
E2721815	0.03	0.00	0.40	0.20	0.01
E2721833	0.09	0.16	5.33	0.97	0.07
WTPC004	0.03	0.13	0.50	0.16	0.04
PDBN 02	0.04	0.59	1.36	0.24	0.04
PDBN 04	0.03	0.39	0.37	0.08	0.02
BLD 3	0.03	0.35	0.53	0.15	0.02
NIST	0.05	0.00	0.00	0.00	0.01
BIR 50mg	22.0	5.41	0.41	0.06	0.02
BIR 25 mg	0.01	0.09	0.01	0.18	0.02
BIR 5 mg	0.02	0.08	0.01	0.41	0.01
BHVO 50 mg	0.04	0.03	0.39	0.11	0.01
BHVO 25 mg	0.02	0.08	0.01	0.49	0.03
BHVO 10 mg	0.02	0.09	0.00	0.84	0.03
BHVO 5 mg	0.01	0.08	0.01	0.78	0.06

THE EFFECT OF MATRIX ELEMENTS ON δ^{65} CU VALUES

δ^{65} Cu **l**iterature values from Liu *et al.* (2013) for matrix induced isotopic shift were analysed using the ThermoFinnigan Neptune Plus MC-ICP-MS at the University of Geosciences, Beijing. The use of a different analytical instrument to this study may vary the offset seen within the samples.

Prevalent matrix elements within the samples included Ti, Na, Mg, and Co, leading to the formation of polyatomic molecules, interfering with Cu isotopic values. The inaccurate δ^{65}Cu of the 50 mg column load of BIR-1a (-3.247 $\pm$0.895‰) is thought to be the direct result of the high abundance of Na (Na/Cu ratio ~22). It has been shown that a Na/Cu ratio of 2.0 leads to δ^{65}Cu offset of -0.08‰ while a ratio of 5.0 results in an offset of -0.18‰ from true values, leading to exponentially more fractionated values with increasing Na abundance (S.-A. Liu *et al.*, 2013). This elemental contamination is not observed in the 50 mg column load of BHVO-2 with minimal contamination, leading to a δ^{65}Cu value of 0.084 ± 0.416‰, which is close to the reported literature value (0.01 ± 0.01‰) (Sossi *et al.*, 2014). It is unclear as to why column load causes contamination in BIR-1a but not BHVO-2. Nonetheless, the isotopic shift to lower δ^{65}Cu values is consistent with the formation of Na polyatomic species $^{23}Na^{40}Ar$ which interfere with ^{63}Cu (S.-A. Liu *et al.*, 2013)

Magnesium has been shown to offset δ^{65}Cu values from +0.3 to +0.5‰ at a Mg/Cu ratio of 1.0 (with a range due to the use of two different mass spectrometers Micromass IsoProbe and a VG Axiom) (Mason, Weiss, Horstwood, Parrish, Russell *et al.*, 2004). Titanium abundances were found to have a direct correlation with δ^{65}Cu values, with 10 mg BHVO-2 yielding the most inaccurate δ^{65}Cu result at 0.706$\pm$ 0.050‰ (Figure 14 &

15). This sample had a Ti/Cu ratio of 0.85. This is in agreement with the literature, which reports that a Ti/Cu ratio of 1.0 will result in a δ^{65}Cu offset of +0.28‰ and that a Ti/Cu ratio of 10 will result in an offset of +3.20‰ from true value (S.-A. Liu *et al.*, 2013).

The interference of Ti on Cu isotopic analysis may occur in a number of ways. The formation of Ti-oxides ($^{16}O^{47}Ti$ and $^{16}O^{49}Ti$) effects ^{63}Cu and ^{65}Cu respectively, however, the natural abundance of ^{47}Ti (7.44%) is higher than ^{49}Ti (5.41%), which would result in a negative offset to δ^{65}Cu with greater interference with ^{63}Cu. Nevertheless, the formation of hydroxides ($^{16}O^{1}H$) of ^{46}Ti and ^{48}Ti would result in a greater influence on ^{65}Cu due to their relative abundances of 73.13% and 8.25%, respectively. This would result in a positive isotopic shift (Li *et al.*, 2009 ; S.-A. Liu *et al.*, 2013). Lastly, the effect of Co contamination is negligible until Co/Cu $\geq$ 10, giving a potential offset of +0.05‰ (S.-A. Liu *et al.*, 2013).

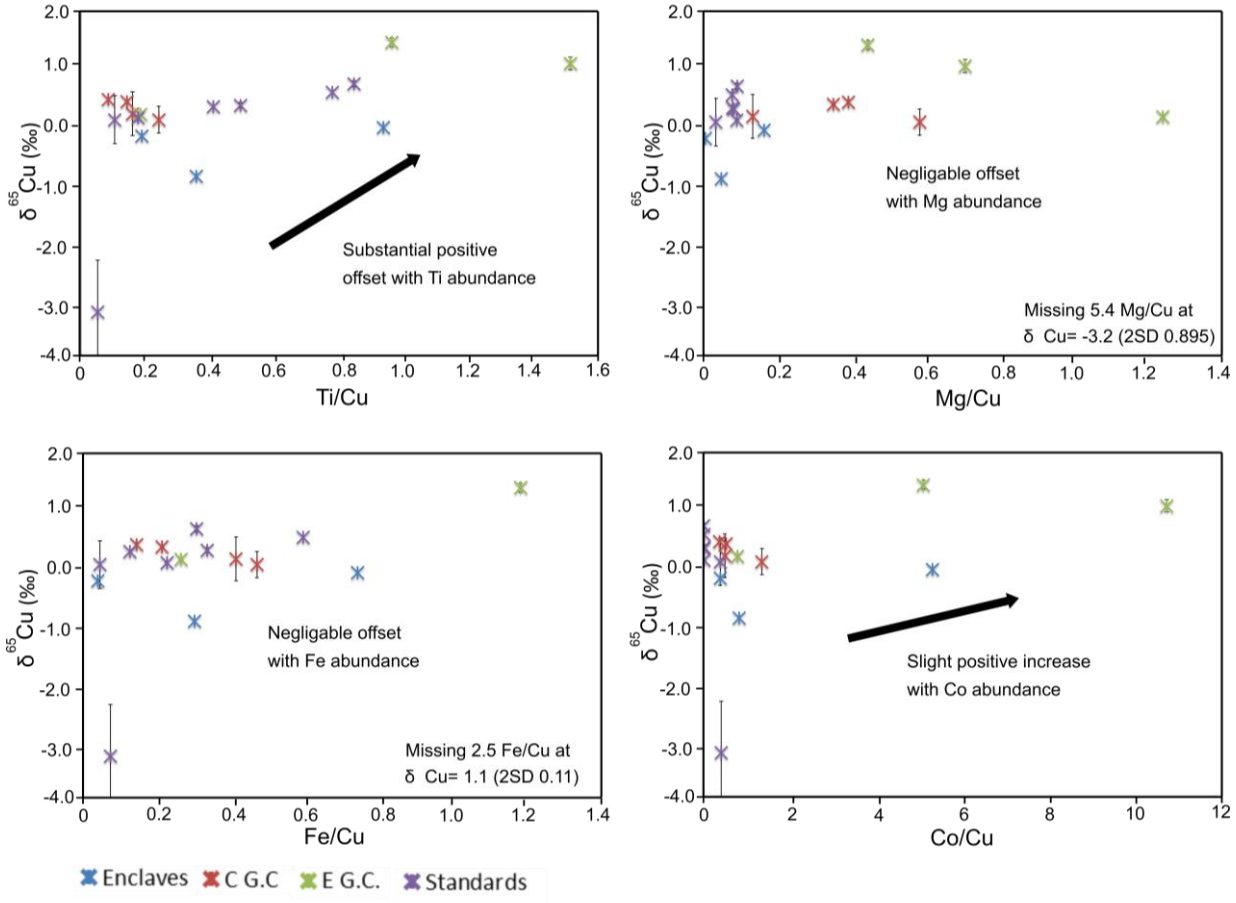

Figure 14 Elemental abundance relative to Cu in the purified fractions.

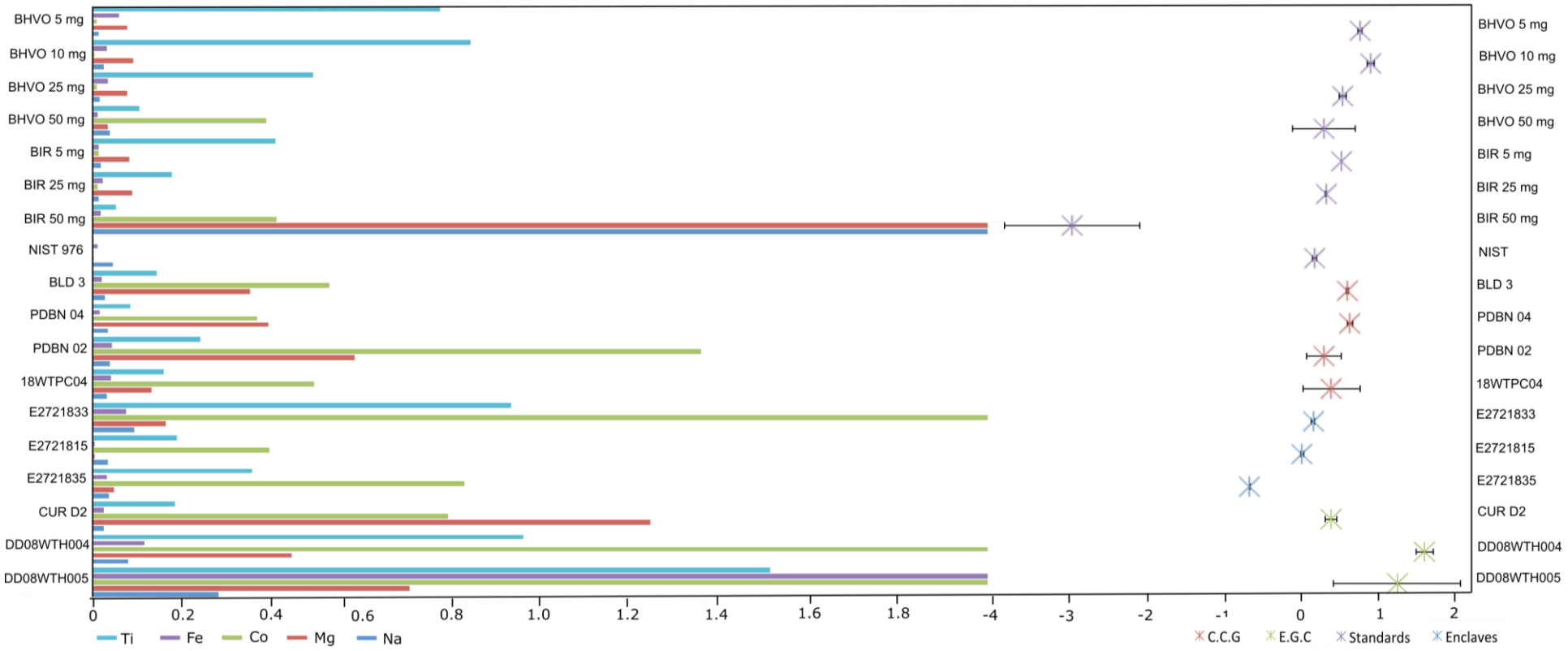

Figure 15 δ^{65} Cu values vs Ti, Co, Mg and Na abundance expressed as a ratio to Cu respective to the samples δ^{65} Cu value. The Cu concentrations for all the samples, including the bracketing sample (NIST 976) is at ~100 ppb. The purified Cu cut of DDH2 did not get analysed after MC-ICP-MS analysis, due to limited sample size.

Given the potential substantial interference by matrix elements, the abundance of matrix elements in Cu cuts must be assessed in each sample prior to calculating δ^{65}Cu values. For this reason all final Cu cuts measured for δ^{65}Cu were also analysed for their trace element abundances by ICP-MS.

Titanium is thought to have the greatest effect (S.-A. Liu *et al.*, 2013). The most pronounced levels of Ti/Cu are in DD08WTH005 (~1.5) followed by DD08WTH004 and E2721833 (~0.9) which would lead to an offset of > +0.28‰ in the former and +0.28‰ in the latter. All other samples range between 0.1-0.41 (Ti/Cu) leading to an offset of 0.00-0.07‰. The highest Na/Cu sample is DD08WTH005 at ~0.3, which would have negligible effect on Cu isotopic values. Most samples contain minimal Fe such that Fe/Cu values are negligible, except for sample DD08WTH005 which has a Fe/Cu of ~2.5. This may have caused a potential offset of -0.1‰ δ^{65}Cu. Furthermore, sample DD08WTH005 is rich in Co and has a Co/Cu value of 10.8 which could cause a potential offset of +0.05‰ δ^{65}Cu (S.-A. Liu *et al.*, 2013).

Titanium induced δ^{65}Cu offset may be corrected for in this specific sample set by examining the values for 5, 10 and 25 mg column load of BHVO-2, exhibiting increasing Ti concentrations within the cut (Figure 14). Direct correlation of Ti with δ^{65} Cu allows for offset to be estimated using δ^{65} Cu values of BHVO-2 (5, 10 and 25 mg column loads) (figure 16). The offset substantially lowers the δ^{65}Cu, by 0.67‰ per Ti/Cu , higher than would be expected with literature values (Table 9) (S.-A. Liu *et al.*, 2013)

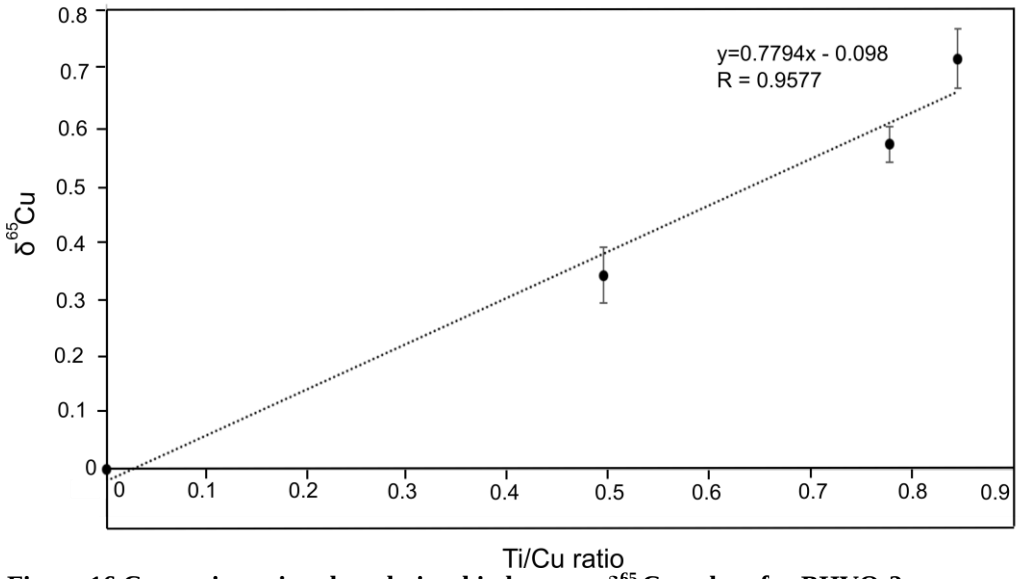

Figure 16 Correction using the relationship between δ^{65} Cu values for BHVO-2

Table 9 Ti/Cu abundance within the purified Cu cuts with the corrected values after the offset.

Sample	Ti	δ^{65} Cu	Corrected δ^{65} Cu
E2721835	0.36	-0.90	-1.17
E2721815	0.19	-0.20	-0.34
E2721833	0.94	-0.05	-0.77
DDO8WTH004	0.96	1.42	0.68
DDO8WTH005	1.51	1.06	-0.11
WTPC004	0.16	0.19	0.07
PDBN 02	0.24	0.08	-0.09
PDBN 04	0.08	0.43	0.38
BLD 3	0.14	0.40	0.30
CUR D2	0.18	0.18	0.04
NIST	0.00	-0.04	-0.03
BIR 50mg	0.05	-3.25	-3.28
BIR 25 mg	0.18	0.12	-0.01
BIR 5 mg	0.41	0.31	0.00
BHVO 50 mg	0.10	0.08	0.01
BHVO 25 mg	0.49	0.33	-0.04
BHVO 10 mg	0.84	0.71	0.06
BHVO 5 mg	0.78	0.56	-0.04

CU ISOTOPES AS A PROXY FOR TRACING MAGMATIC-HYDROTHERMAL PROCESSES

The use of Cu isotopes as a proxy for tracing magmatic-hydrothermal processes is a new field of study and not well understood. Nonetheless several studies suggest that Cu isotopes can be fractionated by hydrothermal processes and that Cu isotopes are not affected by magmatic processes including partial melting and fractional crystallisation (S. A. Liu *et al.*, 2015; Zhao, Xue, Liu, Symons, Zhao *et al.*, 2017). The Cu isotopes of magmatic rocks must therefore reflect their source rock. This is true if (i) the samples used in this study have not assimilated substantial amounts of crustal material, and (ii) samples have not been affected by later hydrothermal overprint. Assuming the Cu isotopes in magmatic rocks directly reflect their source rock, δ^{65}Cu could potentially be used to deduce the extent of mantle metasomatism in the source rocks that gave rise to the Gawler Range magmas. However, prior to interpreting δ^{65}Cu values collected in this study, the potential of crustal contamination and secondary hydrothermal overprint must first be assessed.

EVIDENCE FOR CRUSTAL INTERACTION IN THE SAMPLE SET

The sample set on for which Cu isotopes were obtained represent three spatially separate igneous systems: the Eastern Gawler (E.G.C), Central Gawler (C.G.G) and newly-sampled mafic enclaves within the Gawler Range Volcanics (C.G.C) All samples selected in this study range from ultra-mafic to mafic (Table 5), allowing for the study of Cu isotopes in the least evolved igneous samples of the Gawler Craton.

Variable εNd (–5.5 to + 2.5) as well as depletion in Nb, Ti (Wade *et al.*, 2019), and enrichment in LREE and large ion lithophile elements (LILE), especially in the enclaves, allows for the possibility of crustal contamination. Nevertheless, Wade et al. (2019) demonstrated that fractional crystallisation (FC) and assimilation-fractional crystallisation (AFC) of basaltic samples from Barns deposit (Hiltaba Suite, central Gawler Craton) alone, cannot explain the high abundance of Cr and Ni relative to the amount of SiO_2. This argues against significant crustal input into the magmas that gave rise to the Gawler Range Volcanics and instead suggests that variation in these samples, is, in part, attributed to compositional variation of their mantle source(s) (Wade *et al.*, 2019). The study of Wade et al. (2019), however, did not assess mafic enclaves, which otherwise show significant enrichment in most trace elements relative to other basaltic samples (Figure 6) Unfortunately εNd data was not obtained for these samples. Despite this, their element compositions can be investigated in order to assess potential crustal contamination. The mafic envlaves have a low abundance of MgO, CaO and Fe2O3, and are enriched in K2O, along with a Nb/Y-Zr/Ti plot (figure 5), According to the classification scheme of Pearce (1996) these samples can be classified as andesites rather than as basalts, to suggest these samples are more evolved. As a result of longer residence times in a crustal magma chamber these samples are more likely to be contaminated by crust than the more mafic samples in this study (CGC, EGC). The mafic enclaves also contain higher concentrations of LILE, in particular Ba. These elements are more enriched in the continental crust and therefore melts that have assimilated crust would be expected to be more enriched in LILE than can be accounted for by fractional crystallisation alone. A detailed assessment of fractional crystallisation is beyond the scope of this study. High LILE values alone cannot inconclusively test for

crustal contamination. εNd data would provide a more detailed insight into the fraction of assimilated crust in these mafic enclaves.

EVIDENCE FOR HYDROTHERMAL ALTERATION OF THE SAMPLE SET

Hydrothermal alteration has the potential to introduce secondary Cu into magmatic rocks as secondary sulfides. The resulting δ^{65}Cu of such samples will therefore reflect a mix of magmatic and hydrothermal processes. Rocks within the Gawler Craton are common to have undergone extensive hydrothermal alteration related to IOCG and Au mineralisation within the Gawler province. Nonetheless, all samples selected for Cu analysis appear fresh in whole rock. Analysis of thin sections revealed primary igneous minerals – in particular clinopyroxene and orthopyroxene – are unaltered by secondary minerals such as hematite, chlorite and sericite and their mineral textures are largely preserved.

COPPER AND CRUSTAL INPUT

A direct correlation between the level of mantle input and the tenor of Cu mineralisation has been demonstrated for the IOCG province using Nd isotopes (Skirrow *et al.*, 2007; Skirrow *et al.*, 2018). Nevertheless, no direct correlation can be observed between the εNd and δ^{65}Cu values of samples used in this study (Figure 17). The Nd isotope dataset is however limited and does not include the three enclave, and two E.G.C samples, DD08WTH0004 and DD08WTH0005. This is unfortunate given these samples show

the widest range of δ^{65}Cu values and therefore more data could reveal any potential correlation between εNd and δ^{65}Cu.

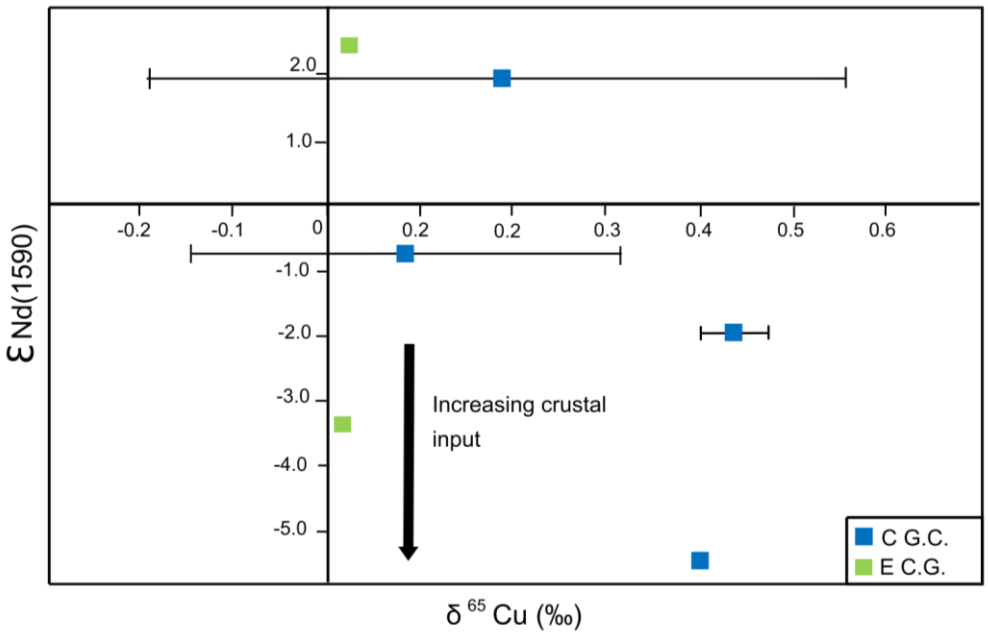

Figure 17 The correlation between Cu isotopic compositions and εNd, an indicator of crustal contamination.

CORRELATIONS BETWEEN δ^{65} CU AND FLUID MOBILE ELEMENTS

A strong inverse correlation with fluid mobile elements: in particular the LILE (Ba, Rb, K), LREE and δ^{65}Cu (figure 18), can be observed in the samples. The enclaves are observed to have negative delta δ^{65}Cu values while the E.G.C samples appear positively fractionated. This relationship between fluid mobile elements and fractionated δ^{65}Cu, more specifically negative fractionation , may indicate a causative relationship between degree of mantle metasomatism and fractionation of δ^{65}Cu values from 0‰ (Figure 18) (S. A. Liu *et al.*, 2015). Alternatively this difference in δ^{65}Cu may simply reflect a heterogeneous mantle source.

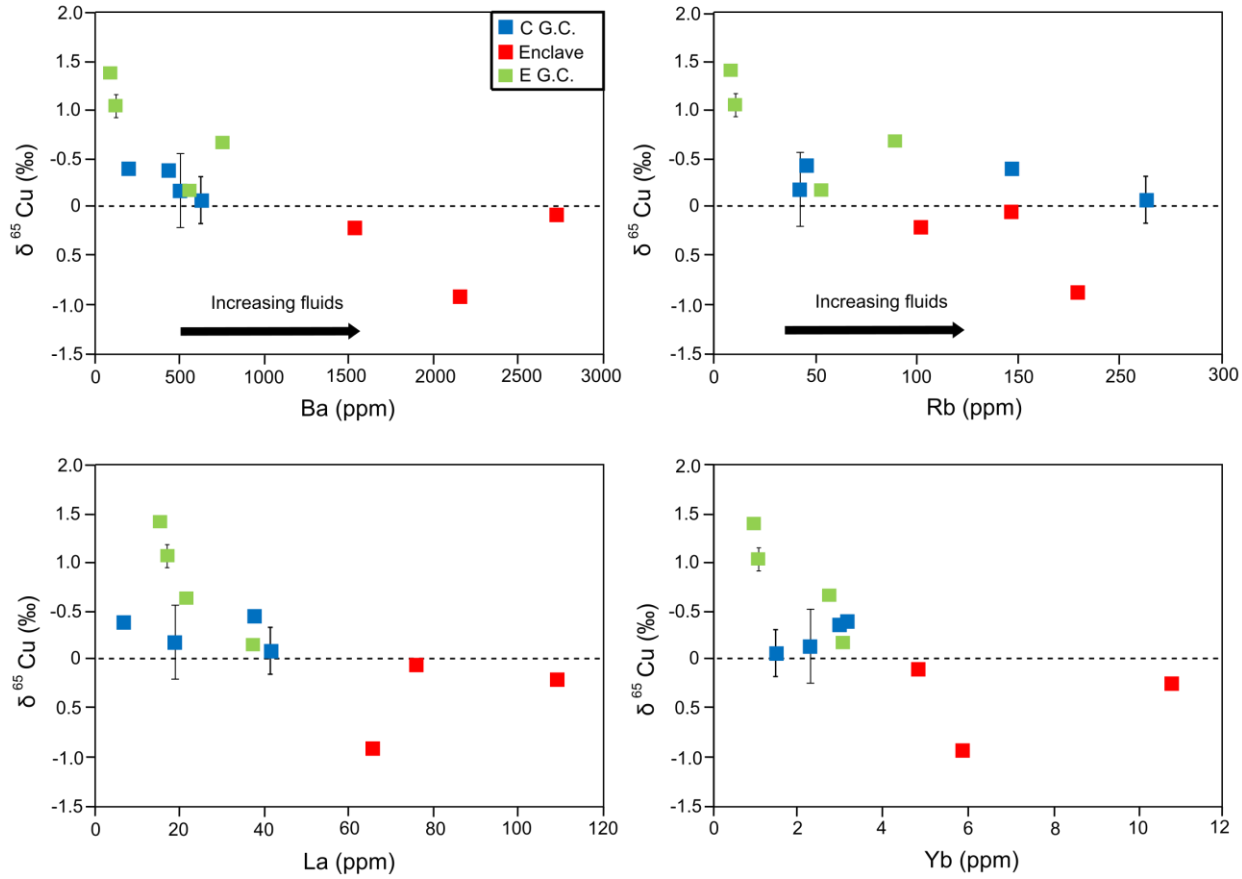

Figure 18 δ^{65} Cu values relative to large ion lithophile elements (LILE) and light rare earth elements (LREE) and heavy rare earth elements (HREE)

SULFIDE MINERALISATION AND IMPACT ON δ^{65} CU

Two sequential crystallisation sequences are observed within the samples of DD08WTH004, DD08WTH005 and CUR D2 via petrology. (1) The lack of pyrite and chalcopyrite inclusions in orthopyroxene with both minerals accumulating interstitial to orthopyroxene and (2) the overprinting of pyrite with chalcopyrite. The former may be indicative of late stage sulfur assimilation through country rock interaction within the magmatic system, or a decrease in the sulfide saturation level of the melt (Ripley & Li,

2013), with either scenario potentially leading to the precipitation of sulfides after orthopyroxene crystallisation.

Sulfur saturation is generally thought to occur during crustal assimilation of S rich country rock. However, closed-system fractional crystallisation may also induce sulfide saturation following 20-40 % fractional crystallisation (Ripley *et al.*, 2013). Sulfide saturation may be triggered in magmatic rocks by either a decrease in temperature or the fO_2 of the silicate melt or a change in the composition of the melt in particular an increase in the fS_2 (Ripley *et al.*, 2013).

The availability of whole rock sulfur concentrations would help to assess the control of sulfide saturation on the abundance of Cu in samples. Although, sulfide saturation may be assessed by other methods, such as petrographical analysis of sulfide textures. The significantly higher abundance of pyrite than chalcopyrite as well as low Cu abundances within the samples 10-60 ppm, indicates that Cu availability was much less than S.

The isotopic values of the samples and petrographic analysis indicates a correlation with the presence of chalcopyrite and positive δ^{65}Cu values (DD08WTH004 = 1.422 ± 0.077‰, DD08WTH005 = +1.057 ± 0.111‰ and CUR D2 = +0.178 ± 0.017‰). However, correcting for Ti reduces the values down to +0.683‰, –0.114‰ and +0.044‰, respectively. As the Ti offset is only an estimate, these values should be treated with caution when interpreting their significance. As previously mentioned, magmatic processes such as crystal fractionation of silicate and oxide minerals should

have had no discernible effect on Cu isotope fractionation (S. A. Liu *et al.*, 2015; Zhao *et al.*, 2017).

In contrast, sulfide saturation and the segregation of sulfide melt is believed to fractionate Cu isotopes. Sulfide melts preferentially remove lighter Cu isotopes (^{63}Cu), shifting the residual magmas to heavier Cu isotopes (S. A. Liu *et al.*, 2015; Zhao *et al.*, 2017). These positive δ^{65}Cu values resemble isotopic values of secondary precipitated Cu-sulfides (Y. C. Zheng, Liu, Wu, Griffin, Li *et al.*, 2018). As a result magmatic sulfide melts will have more negative δ^{65}Cu and the residual silicate melts more positive δ^{65}Cu.

A lack of sulfides in enclave (E2721835), with a Cu abundance of 46 ppm suggests that Cu is unlikely to be hosted in sulfides. The negative δ^{65}Cu values for the mafic enclaves (–0.897‰ to –0.053‰) are opposite to what would be expected if the magmas had previously experienced sulfide saturation (Ripley *et al.*, 2013), indicating another likely method for Cu isotope fractionation. The potential for hydrothermal alteration of mafic enclaves was ruled out, however crustal contamination was not. S-type granites are reported to have negative δ^{65}Cu values within the range of –0.46 to +0.21‰ (Li *et al.*, 2009). Although two of the most negatively fractionated samples are thought to have undergone late stage magmatic differentiation, bringing the δ^{65}Cu range to –0.07 to +0.21‰. This would diminish any isotopic fractionation towards negative δ^{65}Cu values, through assimilation. This could also serve to explain that the degree of LILE element enrichment seen within the enclaves.

The variable δ^{65}Cu values seen within the samples are thought to likely correlate with a heterogeneous mantle source. The sub continental lithospheric mantle (SCLM) below the Gawler Craton, has been shown to be heterogeneous, likely due to previous metasomatic events related to past subduction (reference). Magnetotellurics and seismic tomography have highlighted differences in lithospheric properties of the SCLM under the central and eastern Gawler Craton (Skirrow *et al.*, 2018; Wade *et al.*, 2019). εNd values of mafics throughout the craton are substantially more heterogeneous with no distinct differences seen within the two provinces (Wade *et al.*, 2019). Overall, lower δ^{65}Cu values are seen in the central Gawler craton - through analysis of enclaves and gabbro- relative to eastern Gawler Craton which shows positive δ^{65}Cu values.

FUTURE RESEARCH

The purification of the silicate sample to isolate Copper is a vital component in the accurate determination of δ^{65}Cu. Results from this study suggest that secondary purification, through column chromatography would provide more accurate δ^{65}Cu results. Secondary purification would eliminate matrix elements, in particular those that are known to alter Cu isotopic measurements, such as Ti, Mg, Na, Fe and Co.

It is recommended that the abundance of sulphur within in each sample is determined. This would help identify the relationship between sulfides, Cu and δ^{65}Cu values. Furthermore, thin section analysis of each sample, would further constrain the these relationships, as well as giving an insight into magmatic evolution. Lastly, it is also

recommended that mafic enclaves be analysed for their bulk rock Nd isotopic composition. εNd values for mafic enclaves would help in constraining the level of mantle input in these samples, and help determine whether negative $\delta^{65}Cu$ are a result of crustal contamination or mantle source heterogeneity.

CONCLUSIONS

Effective and vigorous chemical purification of copper is crucial for the determination of $\delta^{65}Cu$ from a silicate matrix. Measurement of eluted Cu solutions by MC-ICP-MS is vital in determining the concentration of matrix elements which may lead to potential interference. The influence of elements such as Mg, Na, Fe, Co, and especially Ti, within purified cuts should receive the most attention, especially in rocks containing a high abundances of these elements relative to Cu.

This study reports the copper isotope data of 11 samples ranging from mafic intrusives (gabbros to andesites) from the Au province (central Gawler Craton) and IOCG province (eastern Gawler Craton), and mafic enclaves from the central Gawler Craton. These samples show variable $\delta^{65}Cu$ values, ranging from -0.897‰ to +1.422‰. Samples from the eastern Gawler Craton show the most positively fractionated $\delta^{65}Cu$ values (+0.69 ± 0.024‰ to +1.422 ± 0.077‰). Enclaves from the central Gawler Craton have the most negatively fractionated $\delta^{65}Cu$ values (-0.053 ± 0.023‰ to -0.897 ± 0.006‰), while intrusives from this region have slightly more positive $\delta^{65}Cu$ values (+0.084±0.23‰ to +0.397±0.011‰). All samples show a lack of hydrothermal

alteration. The sulfides within the samples are therefore interpreted to be magmatic. The presence of magmatic chalcopyrite within the eastern Gawler Craton (IOCG province) samples, appears to correlate with positive δ^{65}Cu. In contrast, the enclaves and samples from the Central Gawler Craton (Au province) are characterised by a lack of chalcopyrite and more negative δ^{65}Cu values.

The positive δ^{65}Cu values observed in the eastern Gawler Craton samples (IOCG province) cannot be explained by current understanding of Cu isotope fractionation during sulfide saturation. The proposed relationship in the literature suggests that magmatic sulfides would preferentially remove heavier over lighter Cu isotopes from the magma, such that magmatic sulfides have more negative δ^{65}Cu values than their parent melt. This trend may instead be attributed to a heterogenous sub-continental lithospheric mantle (SCLM) source. In contrast the negative δ^{65}Cu values of mafic enclaves is possibly caused by assimilation of S-type granitic crust and/or possibly due to a heterogenous SCLM source.

ACKNOWLEDGMENTS

I would like to thank Lucy McGee and Juraj Farkas for their guidance and support on this project. I would like to thank Anthony Reid and Claire Wade and Justin Payne for their help during field work, and Justin especially, for his guidance during multiple analysis on the Neptune. I would like to thank David Bruce for his help within the lab. I also like to thank Jessica Lowczak, for helping me with deepen my knowledge within

geology during the project. I would like to thank Sarah Gilbert and Adelaide Microscopy for constantly helping me during ICP-MS analysis. Finally I would like to thank Liam Scarra

REFERENCES

Allen, S. R., McPhie, J., Ferris, G., & Simpson, C. 2008. Evolution and architecture of a large felsic igneous province in western laurentia the 1.6 ga gawler range volcanics, south australia. *Journal of Volcanology and Geothermal Research, 172*(1-2), 132-147.

Allen, S. R., Simpson, C. J., McPhie, J., & Daly, S. J. 2003. Stratigraphy, distribution and geochemistry of widespread felsic volcanic units in the mesoproterozoic gawler range volcanics, south australia*. *Australian Journal of Earth Sciences, 50*(1), 97-112.

Borrok, D. M., Wanty, R. B., Ridley, W. I., Wolf, R., Lamothe, P. J., & Adams, M. 2007. Separation of copper, iron, and zinc from complex aqueous solutions for isotopic measurement. *Chemical Geology, 242*(3), 400-414.

Enge, G. T., Field, P. M., Jolley, D. F., Ecroyd, H., Kim, H. M., & Dosseto, A. 2016. An automated chromatography procedure optimized for analysis of stable cu isotopes from biological materials. *Journal of Analytical Atomic Spectrometry, 31*(10), 2023-2030.

Foden, J., & Stewart, K. P. 2003. Mesoproterozoic granites of south australia. *Department of Primary Industries and Resources, Report Book*

Gall, L., Williams, H., Siebert, C., & Halliday, A. 2012. Determination of mass-dependent variations in nickel isotope compositions using double spiking and mc-icpms. *J. Anal. At. Spectrom., 27*(1), 137-145.

Hand, M., & Reid, A. 2012. Mesoarchean to mesoproterozoic evolution of the southern gawler craton, south australia. *Episodes 35*(1).

Hand, M., Reid, A., & Jagodzinski, L. 2007. Tectonic framework and evolution of the gawler craton, southern australia. *Economic Geology, 102*(8), 1377-1395.

Lee, C.-T. A., Luffi, P., Chin, E. J., Bouchet, R., Dasgupta, R., Morton, D. M., Le Roux, V., Yin, Q.-z., & Jin, D. 2012. Copper systematics in arc magmas and implications for crust-mantle differentiation.(reports)(author abstract)(report). *Science, 336*(6077), 64.

Li, W., Jackson, S. E., Pearson, N. J., Alard, O., & Chappell, B. W. 2009 The cu isotopic signature of granites from the lachlan fold belt, se australia. *Chemical Geology, 258*(1-2), 38-49.

Liu, S.-A., Li, D., Li, S., Teng, F.-z., Ke, S., He, Y., & Lu, Y. 2013. High-precision copper and iron isotope analysis of igneous rock standards by mc-icp-ms. *J. Anal. At. Spectrom., 29*(1), 122-133.

Liu, S. A., Huang, J., Wörner, G., Yang, W., Tang, Y. J., Chen, Y., Tang, L., Zheng, J., & Li, S. 2015. Copper isotopic composition of the silicate earth. *Earth and Planetary Science Letters, 427*, 95-103.

Mason, T. F. D., Weiss, D. J., Horstwood, M., Parrish, R. R., Russell, S. S., Mullane, E., & Coles, B. J. 2004. High-precision cu and zn isotope analysis by plasma source mass spectrometry
part 1. Spectral interferences and their correction. *Journal of Analytical Atomic Spectrometry, 19*(2), 209-217.

Mathur, R., Titley, S., Barra, F., Brantley, S., Wilson, M., Phillips, A., Munizaga, F., Maksaev, V., Vervoort, J., & Hart, G. 2009. Exploration potential of cu isotope fractionation in porphyry copper deposits. *Journal of Geochemical Exploration, 102*(1), 1-6.

Motta, J. G., Betts, P. G., Thiel, S., Curtis, S., Armit, R., & de souza filho, C. R. 2019. Proxies for basement structure and its implications for mesoproterozoic metallogenic provinces in the gawler craton. *Journal of Geophysical Research: Solid Earth, 124*(3), 3088-3104.

Reid, A. J., & Payne, J. L. 2017. Magmatic zircon lu–hf isotopic record of juvenile addition and crustal reworking in the gawler craton, australia. *Lithos, 292-293*, 294-306.

Ripley, E. M., & Li, C. 2013. Sulfide saturation in mafic magmas: Is external sulfur required for magmatic ni-cu-(pge) ore genesis? *Economic Geology, 108*(1), 45-58.

Romaniello, S. J., Field, M. P., Smith, H. B., Gordon, G. W., Kim, M. H., & Anbar, A. D. 2015. Fully automated chromatographic purification of sr and ca for isotopic analysis. *J. Anal. At. Spectrom., 30*(9), 1906-1912.

Skirrow, R. G., Bastrakov, E. N., Barovich, K., Fraser, G. L., Creaser, R. A., Fanning, C. M., Raymond, O. L., & Davidson, G. J. 2007. Timing of iron oxide cu-au-(u) hydrothermal activity and nd isotope constraints. *Economic Geology, 102*(8), 1441-1470.

Skirrow, R. G., Wielen, S. E., Champion, D. C., Czarnota, K., & Thiel, S. 2018. Lithospheric architecture and mantle metasomatism linked to iron oxide cu-au ore formation: Multidisciplinary evidence from the olympic dam region, south australia. *Geochemistry, Geophysics, Geosystems, 19*(8), 2673-2705.

Sossi, P. A., Halverson, G. P., Nebel, O., & Eggins, S. M. 2014. Combined separation of cu, fe and zn from rock matrices and improved analytical protocols for stable isotope determination. *Geostandards and Geoanalytical Research, 39*(2), 129-149.

Wade, C., Payne, J. B., K. , & Reid, A. 2019. Heterogeneity of the sub-continental lithospheric mantle and 'non-juvenile' mantle additions to a proterozoic silicic large igneous province. *Lithos, 340-341*, 87-107.

Zhao, Y., Xue, C., Liu, S.-A., Symons, D. T. A., Zhao, X., Yang, Y., & Ke, J. 2017. Copper isotope fractionation during sulfide-magma differentiation in the tulaergen magmatic ni–cu deposit, nw china. *Lithos, 286-287*, 206-215.

Zheng, Y.-C., Liu, S.-A., Wu, C.-D., Griffin, W., Li, Z.-Q., Xu, B., Yang, Z.-M., Hou, Z.-Q., & O'reilly, S. 2019. Cu isotopes reveal initial cu enrichment in sources of giant porphyry deposits in a collisional setting. *Geology, 47*(2), 135.

Zheng, Y. C., Liu, S. A., Wu, C. D., Griffin, W. L., Li, Z. Q., Xu, B., Yang, Z. M., Hou, Z. Q., & O'Reilly, S. Y. 2018. Cu isotopes reveal initial cu enrichment in sources of giant porphyry deposits in a collisional setting. *Geology 47*(2), 135-138.

APPENDIX A: EXTENDED METHODS

Rock sawing

A diamond tipped saw was used to remove weathered surface from large rock samples, and to decrease the size of the samples so they can be processed with the rock crusher (<5 cm).

Powdering samples

Rock samples were crushed using the Jaw crusher located at Adelaide University which involved cleaning the instrument with compressed air before wiping all the metal surface of the crusher with isopropanol and filling the catchment tray with fresh paper. Before each sample was processed, quartz chips were milled for 60 seconds within the tungsten ring mill and subsequently cleaned with compressed air, and then wiped with isopropanol. Samples were processed for approximately 100 seconds before being placed on fresh paper and bagged for geochemical analysis.

Reagents, materials, standard solutions, calibration runs and reference materials

All procedures were performed in high efficiency particulate air (HEPA) filtered fume cupboards. Single-distilled acids were used as reagents in the laboratory procedures. Pipette tips were rinsed in 2 Mol L^{-1} HCl and 18.2 MΩ cm purity Mili-Q water. Columns used were BioRad PolyPrep (polypropylene) with a 0.8 cm diameter and 8 cm height were loaded with 1 ml resin. The Prepfast MC system used a new CF-MC-FeZnCd-1000 column during all procedures. Savillex® teflon beakers were cleaned with an initial one hour reflux in recycled 6M HCl followed by a 48 wash bath in 6M HNO3, 48 hour wash bath in 6M HCl and a final 24 hour reflux with 6M HCl. Plastic vials were cleaned by refluxing 6M HCl for 24 hours. Plastic vials were used for all calibration experiments and manual column chromatography.

Calibration using the prepfast

The prepfast was setup according to the setup guide for Sr analysis. Following this the prepFAST MC was set up according to the PrepFAST Fe, Zn, Cu extraction method manual.

1. Open ESI SC Autosampler program
2. Configure prepFAST online
3. Set submethod parameters
4. Adjust parameters to desired settings
5. Start prepFAST

Major and Trace Element Analysis

Digested samples were diluted to 1:1000 for trace elements and 1:80000 for major elements.